October 2011

Improving the Horizontal Transport in the Lower Troposphere with Four Dimensional Data Assimilation

Robert C. Gilliam*, James M. Godowitch, and S Trivikrama Rao

Atmospheric Modeling and Analysis Division, National Exposure Research Laboratory
Office of Research and Development, U.S. Environmental Protection Agency
Research Triangle Park, NC 27711 USA

* *Corresponding author address*. Robert Gilliam, U.S. Environmental Protection Agency (E243-04), 4930 Page Rd., Durham, NC, 27703, USA Tel: +1 919 541 4593, Fax: +1 919 541 1379, E-mail: Gilliam.robert@epa.gov

Abstract

The physical processes involved in air quality modeling are governed by dynamically-generated meteorological model fields. This research focuses on reducing the uncertainty in the horizontal transport in the lower troposphere by improving the four dimensional data assimilation (FDDA) strategy in retrospective meteorological modeling. In particular, characterization of winds in the nocturnal low-level jet and overlying residual layer is crucial to accurately treat regional-scale ozone transport in the key airsheds of the US. Since model errors in wind speed and direction lead to spatial displacements of pollution plumes, observations not routinely used in previous retrospective modeling are introduced into FDDA in an effort to reduce this transport uncertainty. Prior to the main modeling sensitivity, an observational uncertainty analysis was pursued to identify uncertainties in wind speed and direction in the lower 1-km of the troposphere that are inherent in the observational data sets used for data assimilation. Comparisons of observations among various platforms (radar wind profilers, radiosonde soundings and weather radar profiles) in close proximity revealed that an uncertainty of approximately 1.8 m s^{-1} for wind speed and about 20° for wind direction was intrinsic to the observations. In the modeling sensitivities, some minimal improvement of modeled winds within the convective daytime planetary boundary layer (PBL) was found when surface analysis nudging of wind was eliminated. Improvements in the nocturnal jet and residual layer winds at night are demonstrated as a reaction to the use of new observations in the data assimilation in layers above the stable PBL. There is also evidence that the assimilated observations above the convective PBL during the day led to improvements of winds within the PBL, which may relieve the need of all nudging, including surface analysis nudging within the PBL.

Key Words: horizontal transport, observational uncertainty, wind speed and direction errors, nocturnal low level jet, four-dimensional data assimilation (FDDA)

1. Introduction

Regional-scale photochemical grid models, such as the Community Multiscale Air Quality (CMAQ) modeling system (Byun and Schere, 2006), are frequently used for key regulatory decisions, air quality research, air quality forecasting and climate-related studies. In models such as CMAQ, it may be possible to refine chemistry, deposition, diffusion and emissions to a level of near-perfection, but systematic biases in either the strength or direction of the transport winds (disregarding other meteorological parameters) could still lead to poor air quality model solutions. Furthermore, air quality model errors that are driven by meteorology create major difficulties for air quality model developers because of a tendency to attribute these errors to chemistry, aerosol dynamics, photolysis or even other inputs like emissions. Thus, it is important to ensure that main processes, such as lower tropospheric transport, are accurately characterized so the uncertainty in the air quality modeling system inputs can be reduced.

Ozone is one of the criteria pollutants that is affected by regional transport and has an adverse impact on human health, vegetation and ecosystem health (EPA 2004). Processes that lead to the formation and transport of ozone are well understood from the decades of research, which is summarized succinctly in NARSTO (2000) and EPA (2004). Ozone is formed from chemical reactions involving volatile organic compounds and oxides of nitrogen within the well-mixed planetary boundary layer (PBL) during the day in high concentration over major urban and suburban areas. In the evening as the surface cools and the stable boundary layer (SBL) forms, the deep mixed layer of ozone and other pollutants is isolated from the surface in the residual mixed layer. The decoupling of this layer with the rough surface induces an acceleration of wind a few hundred meters above the surface that is often referred to as an inertial oscillation or nocturnal jet (Blackadar, 1957), whose peak magnitude defines the top of the stable boundary layer (SBL). Elevated plumes of pollutants are transported as much as 200-400 km overnight (Blumenthal et al., 1997) by this super-geostrophic nocturnal jet that can be as much as 25 m s^{-1} at an average height of 300-800 m in the eastern US (Zhang et al., 2001; Zhang et al., 2006). As convective mixing resumes the following day, these ozone plumes trapped in the residual layer aloft are mixed down to the surface and combined with locally emitted precursors, further enhancing ozone concentrations (Wolff et al., 1977; Zhang and Rao, 1999; Vukovich and Scarborough, 2005).

Weather, Research and Forecasting (WRF; Skamarock et al. 2008) and CMAQ models are currently the main tools used at the US Environmental Protection Agency (EPA), but they are also used by the broader national and international modeling community. A number of annual meteorological and air quality simulations have been conducted for a variety of applications over the past few years, including the Air Quality Model Evaluation International Initiative (AQMEII; Rao et al., 2011). Persistent biases of wind speed and direction were seen in previous WRF simulations including the annual AQMEII simulation for 2006. These biases and uncertainties in transport need to be minimized with the idea of observation uncertainty in mind. One idea to reduce biases in the wind field is to eliminate Four Dimensional Data Assimilation (FDDA) near the surface or within the PBL as suggested in the past by Zhang et al. (2001), which allows the PBL model to simulate the lower levels of the atmosphere that are influenced by surface fluxes free of any artificial grid FDDA influence. Godowitch et al. (2011), Shafran et al. (2000) and Zhang et al. (2001) found that eliminating FDDA below 2.0 km, 1.5 km, and 1.3 km, respectively, results in a better representation of the nocturnal jet magnitude. However, Godowitch et al. (2011) demonstrated that although the maximum nocturnal jet speed had improved, the wind speed in the residual layer above the jet from approximately 500 to 1000 m or more, where much if not most of the ozone transport occurs at night, was not improved. Godowitch et al. (2011) followed by showing that one technique to improve transport winds in the residual layer was to utilize upper-level observational data from hourly wind profiler sites. Michelson and Seaman (2000) and Nielsen-Gammon et al. (2007) demonstrated that similar wind profiles from different networks could dramatically reduce transport error using limited model domains and time periods.

This study tests a number of FDDA or grid nudging techniques in WRF using more current model analyses and observational datasets in order to identify which methodology has the greatest potential to reduce error and bias in transport aloft. Before this is explored, we thought it would be prudent to examine upper-air observations that are collocated or in close proximity to understand the inherent uncertainty of the observations that are used in the FDDA to better judge meteorological model performance. Zhang et al. (2001), for one, cited the need to understand the uncertainties of different measurements used for evaluation and data assimilation. Then, an examination of a number of model sensitivities that used different FDDA configuration is conducted on a full Continental United States (CONUS) domain for shorter test period. The configuration that demonstrates the most improvement in error and bias is then applied to a full summer model run and is directly compared to the original AQMEII simulations for improvement of the lower-tropospheric transport fields.

2. Methodology

2.1 Models and General Configuration

WRF-ARW version 3.3 was used for all simulations performed here. Gilliam and Pleim (2010) outlined many of the physics options and run procedures for retrospective modeling performed at the US EPA. Here, two simulation periods are examined. The first is a short duration case (August 11-14, 2002) that was examined by Godowitch et al. (2011) who noted that the observed mean daily 8-hr maximum daily ozone concentration in the eastern US over the episode was around 80 ppb, which represents the highest of that summer. This case study is used to determine the most robust FDDA strategy because of its short duration and the weather pattern is nearly identical as the high ozone case discussed in NARSTO (2000). The second simulation covers June through August of 2006. It is a re-run of AQMEII simulation that adopts the most accurate FDDA strategy based on the previous sensitivity tests. The seasonal aspect of this simulation lends more credence to the model evaluation since it covers multiple weather and air quality scenarios.

The modeling domain for all of these simulations was the same and covered the CONUS, most of Canada and Mexico with a horizontal grid spacing of 12 km, 34 vertical layers extending from the surface to the 50 mb pressure level (13 layers below 1 km). This is the exact same domain and WRF configuration used by Godowitch et al. (2011) and Vautard et al. (2011). Among the physics options used for all simulations were the Rapid Radiation Transfer Model Global (RRTMG) long and shortwave radiation (Iacono et al., 2008), Morrison microphysics (Morrison et al., 2008), and the Kain-Fritsch 2 cumulus parameterization (Kain, 2004). For the LSM and PBL models, the Pleim-Xiu land surface model (PX LSM; Xiu and Pleim, 2001; Pleim and Xiu, 2003; Pleim and Gilliam, 2009) and Asymmetric Convective Model version 2 (ACM2) (Pleim, 2007a; Pleim, 2007b) were used.

Nudging/FDDA of full-physics models has a long history dating back to the 1980's (Stauffer and Seaman, 1987) and, in particular, the early 1990's when Stauffer and Seaman (1990), Stauffer et al. (1991) and Stauffer and Seaman (1994) developed the technique to incrementally nudge the state variables of wind, temperature and moisture towards model analyses that are typically generated as initial conditions of US weather forecast models. This has been the US EPA protocol for both the MM5 (Otte, 2008a, Otte, 2008b) and WRF (Pleim and Gilliam, 2009; Gilliam and Pleim, 2010) models with the surface analysis nudging (Stauffer et al.,1991) of wind being applied within the PBL. Otte (2008a) and Otte (2008b) and many other studies (Stauffer et al., 1993; Seaman et al.,1995; Seaman and Michelson, 2000) have argued that FDDA helps improve retrospective meteorological simulations. The studies by Otte (2008a and b) and Barna and Lamb (2000) clearly explain that FDDA improves air quality simulations. This provides some motivation that any improvements in transport or other meteorological fields from these experiments have potential to measurably reduce the uncertainty in air quality models.

2.2 Data Assimilation

An initial evaluation of the annual WRF simulations for AQMEII indicated the meteorological model has a large and persistent bias in 10 m wind speed across the model domain. When this bias was identified, sensitivity tests were performed, which revealed that if surface analysis nudging was eliminated, this 10 m wind speed bias was reduced. Figure 1 presents the domain-wide bias and RMSE of 10 m wind speed for the summer of 2006 AQMEII simulations. Also provided is the sensitivity where the surface analysis nudging was eliminated. While the overall RMSE of wind speed increases around 0.10 m s^{-1} during the day when surface analysis nudging is not used, the model bias decreases from around -0.50 m s^{-1} to near zero for a large part of the diurnal cycle. The impact of surface nudging on model level winds in the lower troposphere, particularly within the convective PBL, will be examined in more detail to determine if its use provides any clear benefit.

In recent years, the sources of routine upper-air observations have increased spatially and temporally. These improvements in data availability present an opportunity to provide high-quality nudging fields that may provide some reduction in model error and bias in the wind fields. The first observation platform is the twice-daily radiosonde soundings (referred to as *RAOB* from here forward) at locations shown in Figure 2. These are typically used in US EPA FDDA simulations and were employed in the annual AQMEII simulation. RAOB soundings have the benefit of being equally spaced across the CONUS, but the weakness is the limited routine sampling at 00 and 12 UTC, which are the times in the US that do not capture the nocturnal jet or diurnal PBL transitions. While the RAOB impact on the quality of the simulated transport fields will be briefly explored, their main use is to judge the uncertainty of the other two observation platforms. RAOB data are considered one of the most reliable measurements as wind speed uncertainty is about 0.2-0.5 m s^{-1} (Velden and Bedka,2009).

In the early 2000's, 915 MHz UHF Doppler radar profilers were made operational in many areas of the US. In addition, about thirty-five 404 MHz UHF Doppler radar profilers have been operating in the central US since the early to mid 1990's. Figure 2 displays the locations of the operational wind profilers during the August 2002 sensitivity study first presented by Godowitch et al. (2011), referred to as *UHF profilers* from here on. The advantage of these data in assimilation is the high vertical (~55 m) and temporal sampling (1 hour and less) in the lower part of the atmosphere; the layer where pollution transport is most important. The wind data has an instrument uncertainty range of ± 1 m s^{-1} and 10 degrees with no minimum wind speed threshold. Certain parts of the US have a high density of these measurements, but the main drawback is that many parts of the US are not well represented and the spacing is highly irregular. However, the areas of the country that have major pollution issues, namely the Mid-Atlantic, northeast US, California and southeast Texas, do have relatively good coverage by these UHF profilers. As an example, Nielsen-Gammon et al. (2007) demonstrated that the high concentration of UHF profilers in Texas dramatically improved MM5 simulations that employed direct hourly observational nudging.

The third observation platform is the Weather Surveillance Radar-1988 Doppler (WSR-88D) radars that use a velocity azimuth display (VAD) algorithm (Lhermitte and Atlas, 1961; Browning and Wexler, 1968; Klazura and Imy, 1993) to derive a vertical profile of the horizontal wind. These Doppler-derived radar observations (referred to as *VAD* profiler from here forward) are a volume scan at sub-hourly intervals that provide radial wind velocity as a function of distance/range, azimuth, and elevation, which the VAD algorithm uses for the horizontal wind speed and direction estimates (Holleman et al., 2008). These VAD data as well as radar reflectivity have been used in recent years in three-dimensional variation data assimilation (3D-VAR) techniques, which are commonly employed in weather forecasting (e.g., Barker et al., 2003; Alpert and Kumar, 2007; Xiao et al., 2008; Benjamin et al., 2010). Michelson and Seaman (2000) were among the first to use these data in retrospective four dimensional data assimilation (FDDA), and found that errors in simulated wind speed and direction, especially below 2000 m, were reduced as a result. As discussed in Michelson and Seaman (2000) and Stauffer and Seaman (1994), VAD observations are comparable to nearby observation platforms that have less measurement uncertainty like in situ RAOB soundings, but there are instances where VAD data are not as reliable. One of the most frequent sources of uncertainty are migrating birds (Gauthreaux et al., 1998), but since this is not as much of a concern in the summer it should not present an issue for this case study, but could be a problem if the data were used for annual simulations. Studies like Gauthreaux et al. (1998), Michelson and Seaman (2000) and Illingworth and Rennie (2009) suggest the uncertainty in VAD wind measurements as compared to nearby RAOB data is around 2.0-3.0 m s^{-1} for wind speed and 20 degrees for wind direction, but these differences were much lower below 1000-2000 m. Holleman (2005) presented a more comprehensive comparison that contained nine months of collocated RAOB and VAD data and found a positive wind speed bias of 0.5 m s^{-1}, standard deviation of VAD-radiosonde difference of 1.5 m s^{-1} and 15 degrees in the layer below 1000 m. Because VAD uncertainty has been proven to increase with height above the surface, in this study, we only assimilate VAD observations below 2000 m.

One key benefit of VAD data unlike the UHF profiler data is the VAD sites have continuous spatial coverage of the US (Klazura and Imy, 1993) because the network was designed to provide comprehensive tracking of severe weather. The site spacing of VAD is equally spaced like the RAOB network as illustrated in Figure 2, but about twice as dense. As a result, Obsgrid was configured with a smaller radius of influence (240 km) than the default that is based of the RAOB site spacing. Another positive characteristic of VAD data as identified in Michelson and Seaman (2000) and is that VAD is not a point measurement like wind profilers and RAOB observations, but more of a volume average around the radar site, which lends itself to grid-based modeling and data assimilation. Regarding the vertical resolution, VAD does not have the vertical sampling density of the UHF profilers or RAOB, but does provide about 3 samples below 1 km, which can resolve features of the nocturnal jet, residual layer and a bulk of the convective PBL. VAD does mark reported wind speeds of less than 1 m s^{-1} as bad, and those were eliminated from the data assimilation and evaluation.

Given the above considerations and our objective of improving the modeled transport in the lower troposphere, a series of sensitivity experiments was designed to determine a new data assimilation strategy. The four-day control or base simulation (BASE) essentially used the existing US EPA modeling protocol (Gilliam and Pleim, 2010) where FDDA/grid nudging is applied above the PBL for all state variables and surface analysis nudging of the 10 m wind is performed within the PBL with stronger influence near the surface that diminishes to zero at the top of the PBL. FDDA fields came from the 42 km Eta Data Assimilation System (EDAS) analyses at 00, 06, 12, and 18 UTC, and a three-hour forecast for the 03, 09, 15, and 21 UTC times. The base

AQMEII simulations for the summer of 2006 has an almost identical configuration, but a more recent 12 km North American Model (NAM) analysis and three-hour NAM forecast was used instead of EDAS. Another minor difference is RAOB observations were blended with the 12 km NAM at 00 and 12 UTC for the three-dimensional grid nudging using the *Obsgrid* objective analysis tool (http://www.mmm.ucar.edu/wrf/users/docs/user_guide_V3/users_guide_chap7.htm). Obsgrid was used to blend 10 m wind observations with the analyses and three-hour forecast fields for the surface analysis nudging of wind. The 10 m wind observations were directly extracted from the ds464.0 global surface observation database archived at National Center for Atmospheric Research (NCAR; http://dss.ucar.edu/datasets/ds464.0).

Sensitivity 1 (SENS1) is the same configuration above, but surface analysis nudging is completely disabled so as to eliminate all nudging within the PBL. Sensitivity 2 (SENS2) will illustrate the impact of eliminating all nudging close to the surface. In the SENS2 simulation, there is no surface analysis nudging or three-dimensional analysis nudging of any state variable below approximately 2000 m. Sensitivity 3 (SENS3) utilizes UHF profiler data to improve the three-dimensional wind analyses using the Cressman objective analysis scheme (Cressman, 1959) in Obsgrid. SENS3 nudging is configured like SENS1 where nudging is completely eliminated within the PBL, but above the PBL, WRF is nudged towards the UHF profiler-influenced Obsgrid re-analysis. While the profiler data will be used to evaluate the error and bias associated with this simulation as a check of the data assimilation veracity, VAD will provide an independent verification at locations away from the profiler sites. It should be noted again that the assimilation uses three hourly re-analyses because of the first-guess analysis interval, but the evaluation considers all hourly samples, so two of three observations are withheld from the assimilation.

Sensitivity 4 (SENS4) utilized VAD wind profiler data only in the assimilation. As with SENS3, the VAD data is blended with the analysis and short-term forecasted wind field on the WRF grid, and no nudging is done in the PBL. This simulation is evaluated against the independent UHF profiler data. Sensitivity 5 (SENS5) employs nudging fields that are a blend of both the VAD and UHF profiler data with the first guess analysis fields and the surface nudging is not performed within the PBL. Sensitivity 6 (SENS6) utilizes UHF, VAD and RAOB observations in the data assimilation. The main test here is to ensure that by adding twice daily RAOB, the model performance relative to VAD and UHF observations is not diminished.

3. Results and Discussion

3.1 Inherent Uncertainty in the Observations

Since RAOB, UHF and VAD profiles, are used in these experiments for data assimilation, it is prudent to inter-compare the various observations in order to quantify the level of observational uncertainty that can be expected. This not only provides a quality control check of the model inputs, but also helps understand the limits of predictability for a model that uses uncertain inputs. The original UHF, VAD and RAOB observations were interpolated from their native height structure to the model levels using a model evaluation tool. This interpolation to the model grid does inject some uncertainty, but the Obsgrid tool also interpolates to model levels for the data assimilation, so these comparisons provide a total uncertainly level that can be expected from this model input. All observational data were then extracted for the summer of 2006 (JJA) at the approximate model levels of 400, 700 and 1000 m. For each observation platform (VAD, RAOB and UHF profiler), sites of the other two platforms were probed for those that fell within a physical site separation distance of 75 km. For each site pair and at each height level, the observations were matched temporally and the average root-mean-square error (RMSE), bias or mean error, and the index of agreement (IOA) among all site pairs were computed for wind speed (Wilks, 1995). The mean absolute error (MAE) and bias were computed for wind direction. For wind direction the MAE was chosen over RMSE because of the greater sensitivity to large difference between the model and observations (Wilks, 1995), which often occurs with wind direction, especially during light wind conditions. These statistics in Table 1 indicate that the UHF and VAD profiler data in close proximity have an approximate error of around 2.1 m s^{-1}; a high wind speed bias nearing 1 m s^{-1} and IOA of around 0.65. The apparent stronger winds in VAD relative to UHF is most likely relate to the minimum VAD wind of 1 m s^{-1} while UHF observations have no minimum wind speed threshold. Table 1 indicates the paired sites within 75 km of each other have an average MAE of about 25 degrees with a minimal bias.

The next two platform inter-comparisons utilize the twice-daily RAOB observations, so the sampling size is much smaller than that in the previous comparison that use hourly VAD and UHF. That said, there are a total of about 100 RAOB sites of twice daily observations over 3 months, so the sample is adequate in a statistical sense. For the RAOB versus UHF comparison (Table 1), 17 site pairs have spacing less than 75 km. The RMSE of wind speed is around 1.6-1.9 m s^{-1} for these sites, which is lower than in the inter-comparison of the UHF profiler and VAD. The overall bias between these sites is smaller (around +/-0.1 m s^{-1} or less) and the IOA is larger (0.7-0.8) than those in the UHF versus VAD comparison. The wind direction (Table 1) for the same paired RAOB-UHF data indicate the average wind direction error is around 20 degrees, which is about 5 degrees lower than the UHF-VAD comparison. The wind direction bias is minimal as well.

The final platform comparison is the RAOB observations with the nearby VAD data. This comparison is more unique than the other two in that many of the RAOB balloon launches are performed at National Weather Service (NWS) offices where the VAD is derived from the weather radars. According to the paired site separation distance, 38 of the 59 site pairs that have a separation distance of 75 km or less are actually collocated or have a spacing of less than one model grid cell. Since there is less uncertainty in the in situ RAOB observations, this comparison provides a strong measure of the representativeness of the VAD data.

Table 1 indicates that the RAOB-VAD pairs have an average RMSE of around 1.9 m s^{-1}. A more specific analysis was done for the 38 collocated sites only and the RMSE for wind speed at 750 m drops slightly from 1.81 to 1.76 m s^{-1}. Like the UHF profiler and VAD comparison, the VAD data has a positive wind speed bias of around +0.5 m s^{-1} when compared to the RAOB. Since the RAOB versus UHF profiler had a smaller bias and error, this may indicate that VAD has systematically higher wind speed and may contain more uncertainty than the other two platforms. Figure 3 provides a more detailed look at the comparison by providing the RMSE of each site pair spatially. The size of the identification dot is inversely proportional to the site separation distance (i.e., largest dot signifies sites are collocated) and the color identifies the RMSE level. The closely-spaced or collocated sites have wind speed RMSE's of 1.50 to 2.25 m s^{-1} while most of the sites with larger separation distances have RMSE's greater than 2.5 - 3.0 m s^{-1}.

The wind direction error in this case is also reduced as the RAOB-VAD pairing distance decreases. The mean absolute error was around 17-20 degrees for closely spaced sites. No large wind direction bias is found. The spatial plot of these errors in Figure 3 indicates very small difference between RAOB and VAD in the central US with many paired data having MAE of 10 degrees or less. These small differences likely result from the climatologically steady southerly flow (Great Plains low-level jet) over relatively flat land results in less wind flow variability on spatial scales of 100 km. The differences are larger in the eastern US (20-25 degrees) and western US (many sites pairs greater than 30 degrees). It is likely that the complex geography is the main cause for difference between closely spaced sites in the western US, and in the eastern US, summers are dominated by the Bermuda High that results in lighter and more variable wind on average, which can result in large wind differences over a small distance.

Others have examined observations in a similar manner. Gauthreaux et al. (1998) compared co-located RAOB and VAD observations at a few sites in Louisiana and found that VAD data that was uncontaminated by bird migration was on average about 2.25 m s^{-1} different (mean absolute error) than the RAOB wind speed. This study was somewhat limited because only a few sites along the Gulf coast were considered and the total number of samples was only nine. Michelson and Seaman (2000) examined 5 collocated sites in the northeast US, which included a total of 90 paired sounding samples and found the RMSE of wind speed to be 3.6 m s^{-1} over the whole 300-3300 m sounding, but much of this error was because of poor agreement above 2000 m. While they did not supply the RMSE of wind speed specifically for levels below 1000m, the mean error or bias was supplied and it was around 0.5 m s^{-1}, which is similar to what has been found here. They also found the RMSE of wind direction was 32 degrees, which is slightly larger than the results seen here. Holleman (2005) showed an almost identical bias and error as found here using a similar comparison, but at only one collocated VAD-RAOB observations. Holleman (2005) included 9 months of data and found the standard deviation of the VAD-RAOB wind speed difference around 1.5 m s^{-1} with a bias of 0.5 m s^{-1} and a standard deviation of wind direction difference of 15 degrees.

3.2 Model Sensitivity Tests

Key questions of these model sensitivities include whether or not the limitation of nudging to the free troposphere only, or a certain height above ground level, will improve transport in the lower 1000 m of the troposphere. Also, can observation platforms such as UHF and VAD, if incorporated into the FDDA analyses, provide some benefit in reducing errors in the lower troposphere wind? To address these questions, the errors of the sensitivities were computed over the 300-1000 m layer at all UHF and VAD sites. This layer was chosen because it covers much of the nocturnal jet and residual layer at night and is representative of the convective PBL during the day, but also because the lowest height of VAD is around 300 m. The layer-averaged change in model error between the sensitivities and the control simulations is the main metric examined here. This metric is plotted spatially, but the domain-wide average values are also provided. To provide an extra layer of information, the layer-average RMSE differences for each sensitivity comparison is plotted in histogram form by day/night and for the two observations platforms (VAD and UHF) in Figure 4.

Figure 5 presents a comparison of SENS1 with the control simulation (BASE) using this layer-average change in model error. The difference between these simulations is the elimination of surface nudging in SENS 1, so no nudging is applied within the PBL. The observation platforms are plotted with different symbols and the table in the lower left provides the collective error of each platform and the simulations. These platform-dependent errors indicate the wind speed RMSE decreased slightly according to both the UHF (2.11 to 2.08 m s^{-1}) and VAD (2.17 to 2.12 m s^{-1}) observations. The spatial map shows RMSE's were reduced or did not change much outside of the southern and southeastern US. Also, out of about 30 sites near the coast, the error was reduced at about 25, which may infer that by eliminating all nudging within the PBL, the model was able to better represent mesoscale circulations associated with the land-water interface. Figure 4 provides a more detailed look at the error differences of wind speed for the SENS1-BASE comparison plotted spatially in Figure 5. The decrease in wind speed error as determined by both VAD and UHF is slightly larger and more common during the day, while the decreases and increases of error are more balanced at night although slightly skewed towards a decrease. This is expected as the 300-1000 m layer is generally above the PBL at night, thus, less impacted by surface analysis nudging.

Wind direction MAE differences are provided in Figure 5 along with the average MAE for each platform and simulation. The domain-wide average MAE for each observation platform shows little change in wind direction error. However, there is considerable site-to-site change in error between the BASE and SENS1, but this is generally limited to a change in error of less than a couple of degrees. Around 18% of the approximate 200 sites have a change in wind direction error of more than 3 degrees and only 6% more than 5 degrees. These changes in error of wind speed and direction suggest that at least some small improvements in transport winds, mostly the magnitude, are gained in this 300-1000 m layer when surface analysis nudging of wind is eliminated and FDDA is only performed above the PBL. As a caution, surface analysis nudging is strongest near the surface and decreases with height. We do not explore the performance at model layers below 300 m, so surface nudging may benefit the simulation in layers closer to the surface. Another point of emphasis is how the average error level of each platform compares to the observational uncertainty in Table 1. At VAD and UHF sites SENS1 approaches the same wind speed and direction errors of the closely located VAD and UHF sites in Table 1.

The next sensitivity experiment (SENS2) eliminates all nudging below 2 km. Figure 6 provides the impact of this sensitivity on the transport error when compared to BASE. At VAD and UHF sites the wind speed error increases slightly overall (2.17 to

2.19 m s^{-1} and 2.11 to 2.15 m s^{-1}, respectively). The distribution of wind speed error differences in Figure 4 indicates large error differences in both the positive and negative directions. At UHF sites, the error differences are balanced at night, but clearly skewed towards larger SENS2 errors during the day. The VAD data suggests a more balanced change in error, both night and day, with a slight skew towards higher SENS2 errors. However, the wind direction error increase for all observation platforms is about 5 degrees on average. The spatial plot indicates many sites have a 3 degree model error increase in many areas of the US; 77% of sites have an increase in error, 54% of sites have an increase of more than 3 degrees and 37% have an increase of more than 5 degrees. The overall small increase in wind speed RMSE and large increase in wind direction errors points to a clear degradation of lower troposphere transport accuracy when nudging is limited to layers above 2000 m.

The third model sensitivity (SENS3) tests the inclusion of UHF wind profiler data in the re-analysis used for grid nudging and is compared to SENS1. The only difference tested is the use of UHF profiler observations in the assimilation above the PBL. Figure 7 and the histograms in Figure 4 indicate that as expected, when UHF data is used in the nudging, and then used to evaluate the model, a dramatic decrease in wind speed error is clearly evident. The RMSE decreases from 2.08 to 1.78 m s^{-1} at UHF sites. At the independent VAD sites there is also a decrease in RMSE, but much smaller with an overall decrease from 2.12 to 2.10 m s^{-1}. With that said, the reduction of error at UHF sites does translate to more significant improvements at nearby VAD sites with the exception of a few cases. In the northeast US, every decrease in error at UHF sites is matched with a -0.1 to -0.5 m s^{-1} change in error at the nearby VAD sites. This is also mostly true in the other areas of the US where UHF sites exist (i.e., central Plains, upper Midwest US and the West Coast). The histograms of wind speed error change in Figure 4 for the SENS3-SENS1 comparison illustrates the large reduction of error as determined by the UHF observations both day and night. One important result to expand upon is the clear decrease during the daytime. Since the 300-1000 m layer examined here is most often within the PBL where direct nudging has been eliminated, this error decrease within the PBL is a response to UHF data being assimilated above the PBL. The error changes as determined by VAD is not as clear at the smallest change bins of the histogram, but at the larger change bins the error decrease is more frequent, both day and night, than error increases. These largest error decreases in the histograms are at those VAD sites near the UHF sites shown in Figure 7. Wind direction error change in Figure 7 does not show much difference in an overall sense at the VAD sites (both 23 degrees), but at UHF sites there was a clear decrease from 26 to 22 degrees. The largest decreases in wind direction error, as determined by VAD, were in regions where UHF data was assimilated.

The fourth sensitivity test (SENS4) examines the change in model error when VAD wind profile observations are exclusively incorporated into the FDDA analysis used for grid nudging. The main focus here is the change in model error as judged by independent hourly UHF observations. Figure 8 and Figure 4 provides the comparison between SENS4 and SENS1. The mean RMSE and the spatial representation obviously show the large model error decreases at VAD sites in response to a portion observations being directly used in the data assimilation, with an overall error decrease from 2.12 to 1.82 m s^{-1}. The mean RMSE of the independent UHF sites decreases, to a lesser extent, than VAD, from 2.08 to 2.03 m s^{-1}. An inspection of the spatial wind speed RMSE differences (Figure 8) reveals that in almost every case, UHF sites that are located near VAD sites report a reduction of WRF error. In fact, across the eastern US only a couple of UHF profiler sites independently confirm an increase in error, and most have the same level of error reduction as VAD sites in the same region. Figure 4 depicts the error change at UHF sites within this 300-1000 m layer is skewed towards sizable error reduction at night with more balanced binned differences during the day. This is strong evidence that the use of VAD alone improves the simulated nocturnal wind speed in this important 300-1000 m layer above ground level. This may have been less clear in the previous sensitivity because VAD unlike UHF is more evenly spaced and widespread.

Wind direction error is reduced at VAD sites overall, with a reduction from 23 to 21 degrees over the 300-1000 m layer. The spatial plot verifies that this decrease of wind direction error at VAD sites is consistent across the domain, with the largest improvements along the West Coast and southern US. As an independent dataset, the UHF sites do not show a decrease in error when averaged, but the spatial plot reveals that very few of the UHF sites have a wind direction error difference more than a couple of degrees. A histogram of these error differences not shown here indicates balanced error differences with only 12% of the wind direction error differences of more than 3 degrees.

SENS5 includes both VAD and UHF profiler data in the objective re-analysis used for nudging, and compared here to SENS1 (Figure 9). The key question is whether or not the inclusion of both platforms maintains the error reduction found when each is included separately. A reduction of wind speed error is noted at most VAD and UHF sites as one would expect. The average RMSE at UHF sites is reduced from 2.08 to 1.73 m s^{-1} and at VAD sites the error is reduced from 2.12 to 1.83 m s^{-1}. These average wind speed RMSE's for each platform in SENS5 are about the same or even lower as in SENS3 (UHF 1.78 m s^{-1} in SENS3 versus 1.73 m s^{-1} in SENS5) and SENS4 (VAD 1.82 m s^{-1} in SENS4 versus 1.83 m s^{-1} in SENS5), where these observation were exclusively incorporated. This same conclusion is true for the wind direction. Overall the wind direction error, as determined by VAD and UHF, is reduced by the SENS5 configuration when compared to SENS1, and the overall SENS5 VAD wind direction error is the same as SENS4 where VAD was used exclusively. Wind direction error at the UHF sites is decreased in SENS5 compared to SENS1, and the same as SENS3 where UHF was used exclusively. Figure 4 indicates the distribution of wind speed error differences are skewed almost exclusively towards error reduction by SENS5 in nearly all cases. This is expected at night, but the clear improvements during the day when this 300-1000 m layer is frequently within the PBL where nudging has been eliminated is strong proof again that improved transport above the PBL will translate to improved transport within the un-nudged convective PBL, more so than using 10 m wind analyses to nudge near-surface wind to levels upward in the PBL.

The final sensitivity (SENS6) explores the error change when VAD, UHF and finally the RAOB are used in the data assimilation. SENS6 is compared against SENS5 instead of SENS1 in this case to understand whether the addition of twice-daily RAOB will degrade the model relative to VAD and UHF. The average error for each platform in Figure 10 indicates very little degredation when RAOB are added to the data assimilation. The UHF error does increase slightly from 1.73 m s^{-1} in SENS5 to 1.79 m s^{-1} in SENS6, but with the more widespread VAD sites, errors remains about the same (1.82 m s^{-1} versus 1.83 m s^{-1}). The distribution in Figure 4 indicates the much smaller error changes as a result of RAOB than in the other sensitivities. Wind direction error differences in Figure 10 are also small where at 95% of the VAD and UHF sites the error difference is less than 1 degree. The overall error levels of wind speed (approx. 1.8 m s^{-1}) and wind direction (approx. 20 degrees) in SENS6 are comparable to the level inherent in the observations (Table 1), which infers the direct data assimilation is working well at not only the analysis times, but also in between. Furthermore, the assimilation of these data above the convective PBL improves the winds within the PBL potentially without the need of an artificial surface analysis nudging algorithm. The full summer case will explore the use of this SENS6 configuration in a seasonal simulation.

3.3 Summer 2006 Case

SENS6 was the configuration determined to provide the lowest overall wind speed and direction error. For this longer-term 2006 case, WRF was configured identically to SENS6 and executed for the June 1 through August 31, 2006 period. The main interest here is how the wind errors in the 300-1000 m layer compare with the original AQMEII simulation (Vautaurd et al., 2011) that was configured similarly to BASE. Figure 11 provides the layer-averaged wind speed RMSE and bias for both simulations, as well as the MAE for wind direction. The domain-wide error and bias computed for each observation platform is also provided. The wind speed error is visibly reduced, or about the same, at all profiler sites. The average RMSE of the model at VAD sites decreased from 2.14 to 1.74 m s^{-1}, which is similar to the error reduction seen between SENS1 and SENS6 (Figure 5 and Figure 10). The overall RMSE as determined from all the UHF observations was also reduced from 2.07 to 1.84 m s^{-1} because of the new assimilation; again this is similar to the reduction seen in the sensitivity tests. Spatially, the error reduction occurs across the whole domain, but is most evident across the eastern half of the US. Error levels of the AQMEII simulation were generally in the 1.8 to 2.5 m s^{-1} range in the eastern US. The new assimilation technique reduced those transport errors to 1.2 to 2.0 m s^{-1}. Also of importance, the spatial distribution of error illustrates that the new simulation has an error that is regionally consistent, even across platforms. Almost every UHF site, for example, has a similar level of error as the nearest VAD site, and those errors are similar to the observational uncertainty documented in Table 1.

Wind speed bias is presented in Figure 11. The platform-averaged bias indicates a large reduction from -1.34 to -0.75 m s^{-1} at VAD sites and from -0.44 to -0.21 m s^{-1} at UHF sites. The observational uncertainty analysis indicated that VAD had around a +0.5 m s^{-1} bias when compared to both UHF and RAOB. The use of these VAD data in assimilation essentially increases the domain-wide wind speed in the lower troposphere since VAD sites are evenly spaced, and hourly.

A consistent reduction of wind direction error is also apparent (Figure 11) across the model domain where the overall MAE is reduced by 2-4 degrees at both VAD and UHF sites. Like the RMSE of wind speed, the wind direction errors are much more regionally consistent within the VAD and UHF networks, but also across observation platforms. All UHF and VAD sites in the southeast US, for example, have an MAE of 20-25 degrees. In the northeast US and especially central US, the wind direction errors are even lower with values between 10 and 20 degrees with many sites with model errors as low as 10-15 degrees. The wind direction errors are more variable in the western US, but sites from different observation platforms, in the same vicinity, have about the same level of error. A level of error in the 20 to 25 degree range is approaching the inherent uncertainty levels found in the observations (Table 1). Furthermore, the large number of sites that have model errors on the order of 10-20 degrees indicate the model is actually at or below the uncertainty levels of the observations, which is in the range of 17-20 degrees at collocated RAOB and VAD sites.

Figure 12 provides a final examination of model performance over the diurnal cycle. The RMSE and bias of wind speed and MAE of wind direction are partitioned into far eastern (see Figure 2 for sites) and far western US (see Figure 2 for sites). The model performance is computed using all VAD and UHF profilers in those regions at the 400, 700 and 1000 m levels. Model error and bias of wind speed and error of wind direction are reduced at all levels at all times of the day in both regions. During the day (~12-23 UTC) in the eastern US, the wind speed error is reduced by 0.25 m s^{-1} and the bias decreases from -1.25 m s^{-1} to less than -0.5 m s^{-1}. Wind direction errors were also decreased, but only by a few degrees during the daytime. There is less of an improvement in the western US during the daytime, but some model performance gains are apparent.

These results provide some support to the idea that the representation of the daytime convective boundary layer can be improved if the geostrophic forcing above the PBL is improved through the use of the VAD and UHF observations in the FDDA if the surface-based nudging in the PBL is relaxed or eliminated. An argument against this claim could be that these observations used in the evaluation are being used in the nudging. This is only minimally true as the 400, 700 and 1000 m layers are typically within the PBL during the daytime, so in these experiments those UHF and VAD observations within the PBL are not used in the nudging. At night, these layers are generally above the PBL, so improvement shown here are a direct result of the data assimilation. Another point, the observations are used through the assimilation of 3-hourly re-analyses while the evaluation uses the entire database of hourly observations, so even between analyses the model performance is shown to improve in Figure 12. At night specifically, the wind speed RMSE decreases by around 0.3 to 0.5 m s^{-1} in both regions and the wind speed bias generally improves. Wind direction error is reduced at night much more than the day with decreases of error on the order of 5-8 degrees in both regions. These results at night provide some confidence that nocturnal transport within the nocturnal jet and residual layer have been improved with the new data assimilation.

4. Conclusions

The focus of this research is improving regional-scale transport of pollutants in air quality models by reducing the uncertainty in the simulated wind speed and direction in the lower 1000 m of the atmosphere where pollution transport is most important. The means of these model improvements was explored through several sensitivity experiments.

To establish a baseline for the lower bound for the errors, an observational uncertainty analysis was first presented where three observation platforms were inter-compared (UHF profiler, VAD profiles and radiosonde) by pairing the closely located sites from different platforms. In particular, the comparison of VAD with nearby radiosonde data is the best example as a number (38) of VAD sites are actually collocated with the radiosonde balloon soundings. There were also about 34 VAD sites that were in close proximity to UHF profiler sites. The RMSE in wind speed between these collocated or closely spaced sites is approximately 1.8 m s^{-1} (+/- 0.2 m s^{-1}), and the average absolute differences in the wind direction is near 20 degrees. This uncertainty in wind, as one would expect, is greater in areas of complex terrain and near coastal areas where local sea and land breezes dominate. In the future, the development of site specific uncertainty levels and directly comparing that to model errors determined at these sites would advance this type of uncertainty analysis.

The sensitivity analysis examined a four day case study in August 2002 and found that surface nudging did not substantially improve and in some cases increased wind speed and direction errors in the 300-1000 m layer during the day. The most spatially-consistent improvement in wind speed and direction in the 300-1000 m layer was the sensitivity that included all observation platforms in the reanalysis used for nudging above the PBL. The two sources of hourly observation, VAD and UHF profilers, were injected into the reanalysis separately as well as combined. The simulation that used the UHF observations, for example, was evaluated using the independent VAD wind observations and vice versa. The independent evaluation in both cases showed that model error as determined by VAD observations decreased in areas near the UHF assimilated sites, in almost every case. When both sources of observations were used, the level of error was about the same as cases where they were used separately. This level of model error with respect to UHF and VAD observations did not degrade when RAOB observations were incorporated. Furthermore, the level of model error in the sensitivity that used all observations approaches that found in the observational uncertainty analysis.

The model configuration determined by the sensitivity analysis to contain the least amount of error was applied to a longer three month WRF simulation covering the summer of 2006. This experimental result was then compared to those from a previous simulation done for the AQMEII project. The comparison shows a clear improvement in lower tropospheric transport wind, which is directly linked to the new data assimilation. Results of diurnal wind speed and direction statistics for both the eastern and western US indicate that the use of the new observations are key in reducing the uncertainty in wind speed/direction at night around the nocturnal jet core and throughout the residual layer. A clear improvement was also noted in the mid and lower PBL during the day, which would support the idea that the removal of all nudging in the PBL can improve the representation of the convective PBL as long as these VAD and UHF observations are used to improve the characterization of the geostrophic wind at the top of the PBL. Conceptually, this is a preferred modeling methodology as the PBL and LSM are allowed to interact without any artificial nudging influence. Furthermore, the level of error of both wind speed and direction is in the range of the uncertainty of the observations, which implies an evaluation limit or level of predictability might have been reached with this particular simulation. Any further reduction of model error would likely have to originate from reducing the uncertainty of the observations that are input to the data assimilation, except in the case where the PBL and LSM parameterizations are improved.

Observation uncertainty is an important consideration in any model evaluation study. Deterministic models can never reach perfection and they contain inherent errors that are partly a function of inputs, especially when data assimilation like that done in retrospective simulations is performed. Evaluation results should be viewed in this context. Other sources of meteorological wind observations should be explored including in-flight, take-off and landing observations from aircraft as well as satellite derived wind data. The recent study Benjamin et al. (2010) similarly explored the use of a number of the more recent observation platforms including UHF wind profilers, VAD and RAOB, but they also examined the impact of aircraft and various satellite derived observations. An exploration of these data will be a next step of this evolving research.

Acknowledgements

NOAA / ESRL GSD is recognized for the development and maintenance of the MADIS archive of wind profiler measurements used in our evaluation. The VAD data for this study are from the Research Data Archive (RDA) which is maintained by the Computational and Information Systems Laboratory (CISL) at the National Center for Atmospheric Research (NCAR). NCAR is sponsored by the National Science Foundation (NSF). The original data are available from the RDA (http://dss.ucar.edu) in dataset number ds337.0. The U.S. Environmental Protection Agency through its Office of Research and Development funded and a managed the research described here. Although it has been subjected to Agency review and clearance, it does not necessarily reflect the views and policies of the Agency.

References

Alpert, J. C., V. K. Kumar, 2007: Radial Wind Super-Obs from the WSR-88D Radars in the NCEP Operational Assimilation System. *Mon. Wea. Rev.*, **135**, 1090–1109.

Barker, D. M., W. Huang, Y.-R. Guo, and A. Bourgeois, 2003: A Three-Dimensional Variational (3DVAR) Data Assimilation System For Use With MM5. NCAR Tech Note, NCAR/TN-453+STR, 68 pp. (Available from UCAR Communications, P.O. Box 3000, Boulder, CO, 80307.)

Barna, M., and B. Lamb, 2000: Improving ozone modeling in regions of complex terrain using observational nudging in a prognostic meteorological model. *Atmos. Environ.*, 34, 4889–4906.

Benjamin, S. G., B. D. Jamison, W. R. Moninger, S. R. Sahm, B. E. Schwartz, T. W. Schlatter, 2010: Relative Short-Range Forecast Impact from Aircraft, Profiler, Radiosonde, VAD, GPS-PW, METAR, and Mesonet Observations via the RUC Hourly Assimilation Cycle. *Mon. Wea. Rev.,* 138, 1319–1343.

Blackadar, A. K., 1957: Boundary layer wind maxima and their significance for the growth of nocturnal inversions. Bull. Amer. Meteor. Soc., 38, 283–290.

Blumenthal, D.L. Lurmann, F., Kumar, N., Dye, T., Ray, S, Korc, M., Londergan, R., Moore, G., 1997. Transport and mixing phenomena related to ozone exceedances in the northeast U.S. EPRI Report TR-109523, Electric Power Research Institute, Palo Alto, CA.

Browning, K. A., R. Wexler, 1968: The determination of kinematic properties of a wind field using Doppler radar. *J. Appl. Meteor.*, **7**, 105-113.

Byun, D., Schere, K. L., 2006. Review of the governing equations, computational algorithms, and other components of the Models-3 Community Multiscale Air Quality (CMAQ) modeling system. *Applied Mechanics Reviews*, 59, 51-77.

Cressman, G. P., 1959: An Operational Objective Analysis System. *Mon. Wea. Rev.*, **87**, 367–374.

EPA, 2004 U.S. EPA, The Ozone Report: Measuring Progress Through 2003, Office of Air Quality Planning and Standards, the U.S. Environmental Protection Agency, EPA-454-K-04-001, Research Triangle Park, NC (April, 2004).

Gauthreaux, Sidney A., David S. Mizrahi, Carroll G. Belser, 1998: Bird Migration and Bias of WSR-88D Wind Estimates. *Wea. Forecasting*, **13**, 465–481.

Gilliam, R. C., J. E. Pleim, 2010: Performance Assessment of New Land Surface and Planetary Boundary Layer Physics in the WRF-ARW. *J. Appl. Meteor. Climatol.*, **49**, 760–774.

Godowitch, J. M., R. C., Gilliam and S T. Rao, 2011: Diagnostic Evaluation of the Chemical and Transport Processes in a Regional Photochemical Air Quality Modeling System. *Atmos. Environ.* 45, 3977-3987.

Holleman, I., 2005: Quality Control and Verification of Weather Radar Wind Profiles. *J. Atmos. Oceanic Technol.*, **22**, 1541–1550.

Holleman, I., Gasteren, H., Bouten, W., 2008: Quality Assessment of Weather Radar Wind Profiles during Bird Migration. *J. Atmos. Oceanic Technol.*, **25**, 2188–2198.

Iacono M.J., J.S. Delamere, E.J. Mlawer, M.W. Shephard, S.A. Clough, and W.D. Collins, Radiative forcing by long-lived greenhouse gases: Calculations with the AER radiative transfer models, *J. Geophys. Res.*, 113, D13103, doi:10.1029/2008JD009944, 2008.

Illingworth, A., and S. Rennie, 2009: Estimating winds using radar returns from insects. Proceedings of the 8th International Symposium on Tropospheric Profiling, ISBN 978-90-6960-233-2 Delft, The Netherlands, October 2009.

Kain, J. S., 2004: The Kain-Fritsch convective parameterization: An update. *J. Appl. Meteor.*,43, 170–181.

Klazura, Gerard E., David A. Imy, 1993: A Description of the Initial Set of Analysis Products Available from the NEXRAD WSR-88D System. *Bull. Amer. Meteor. Soc.*, **74**, 1293–1311.

Lhermitte, R.H., and D. Atlas, 1961: Precipitation motion by pulse Doppler. *Preprints Ninth Radar Meteorology Conf.*, Kansas City, Amer. Meteor. Soc., 218-223.
Lin, C. ,2008. Impact of downward mixing ozone on surface ozone accumulation in southern Taiwan. *Journal of Air and Water Management Association*, 58:562-579.

Michelson, S. A., N. L. Seaman, 2000: Assimilation of NEXRAD-VAD Winds in Summertime Meteorological Simulations over the Northeastern United States. *J. Appl. Meteor.*, **39**, 367–383.

Morrison, H., G. Thompson, V. Tatarskii, 2009: Impact of Cloud Microphysics on the Development of Trailing Stratiform Precipitation in a Simulated Squall Line: Comparison of One- and Two-Moment Schemes. *Mon. Wea. Rev.*, 137, 991–1007.

NARSTO, 2000. An Assessment of Tropospheric Ozone Pollution —A North American Perspective. NARSTO Management Office (Envair), Pasco, Washington. http://narsto.org/

Nielsen-Gammon, J. W., R. T. McNider, W. M. Angevine, A. B. White, and K. Knupp, 2007: Mesoscale model performance with assimilation of wind profiler data: Sensitivity to assimilation parameters and network configuration, *J. Geophys.Res.*, **112**, D09119, doi:10.1029/2006JD007633.

Otte, T. L., 2008a: The Impact of Nudging in the Meteorological Model for Retrospective Air Quality Simulations. Part I: Evaluation against National Observation Networks. *J. Appl. Meteor. Climatol.*, **47**, 1853–1867.

Otte, T. L., 2008b: The Impact of Nudging in the Meteorological Model for Retrospective Air Quality Simulations. Part II: Evaluating Collocated Meteorological and Air Quality Observations. *J. Appl. Meteor. Climatol.*, **47**, 1868–1887.

Pleim, J. E., and A. Xiu, 2003: Development of a Land-surface Model. Part II: Data Assimilation. *J. Appl. Meteor.*, **42**, 1811–1822.

Pleim, J. E., 2007a: A Combined Local and Nonlocal Closure Model for the Atmospheric Boundary Layer. Part I: Model Description and Testing. *J. Appl. Meteor. Clim.*, **46**, 1383–1395.

Pleim, J. E., 2007b: A Combined Local and Nonlocal Closure Model for the Atmospheric Boundary Layer. Part II: Application and Evaluation in a Mesoscale Meteorological Model. *J. Appl. Meteor. Clim.*, **46**, 1396–1409.

Pleim, J. E., and R. Gilliam, 2009: An Indirect Data Assimilation Scheme for Deep Soil Temperature in the Pleim–Xiu Land Surface Model. *J. Appl. Meteor. Climatol.*, **48**, 1362–1376.

Ryan, W.F, Doddridge, Dickerson, R.R., Morales, R.M., Hallock, K.A., Roberts, P.T., Blumenthal, D.L., Anderson, J.A., Civerolo, K.L., 1998. Pollutant transport during a regional O3 episode in the mid-Atlantic states. *Journal of Air and Waste Management Association*, 48:786-797.

Shafran, P.C., Seaman, N.L. and Gayno, G.A.: 2000, Evaluation of numerical predictions of boundary-layer structure during the Lake Michigan Ozone Study (LMOS), *J. Appl. Meteorol.* **39**, 412–426.

Seaman, Nelson L., David R. Stauffer, Annette M. Lario-Gibbs, 1995: A Multiscale Four-Dimensional Data Assimilation System Applied in the San Joaquin Valley during SARMAP. Part I: Modeling Design and Basic Performance Characteristics. *J. Appl. Meteor.*, **34**, 1739–1761.

Seaman, Nelson L., Sara A. Michelson, 2000: Mesoscale Meteorological Structure of a High-Ozone Episode during the 1995 NARSTO-Northeast Study. *J. Appl. Meteor.*, **39**, 384–398.

Seaman, N. L., 2000: Meteorological modeling for air-quality assessments. *Atmos. Environ.*, 34, 2231–2259.

Skamarock, W. C., J. B. Klemp, J. Dudhia, D. O. Gill, D. M. Barker, M. G. Duda, X-Y Huang, W. Wang, and J. G. Powers, 2008: A description of the advanced research WRF version 3. NCAR Tech Note NCAR/TN 475 STR, 125 pp. [Available from UCAR Communications, P.O. Box 3000, Boulder, CO 80307.]

Stauffer, D.R., and N.L. Seaman, 1987: A real-data numerical study and four-dimensional data assimilation application for mesobeta-scale flow in complex terrain. *Proc. Symp. Mesoscale Analysis and Forecasting*, Vancover, British Columbia, Canada. International Association of Meteorology and Atmospheric Physics (IAMAP), 533-538.

Stauffer, David R., Nelson L. Seaman, 1990: Use of Four-Dimensional Data Assimilation in a Limited-Area Mesoscale Model. Part I: Experiments with Synoptic-Scale Data. *Mon. Wea. Rev.*, **118**, 1250–1277.

Stauffer, David R., Nelson L. Seaman, Francis S. Binkowski, 1991: Use of Four-Dimensional Data Assimilation in a Limited-Area Mesoscale Model Part II: Effects of Data Assimilation within the Planetary Boundary Layer. *Mon. Wea. Rev.*, **119**, 734–754.

Stauffer, David R., Nelson L. Seaman, 1994: Multiscale Four-Dimensional Data Assimilation. *J. Appl. Meteor.*, **33**, 416–434.

Rao, ST, S. Galmarini, K. Puckett, 2011: Air Quality Model Evaluation International Initiative (AQMEII): Advancing the State of the Science in Regional Photochemical Modeling and Its Applications. *Bull. Amer. Meteor. Soc.*, **92**, 23–30.

Vautard, R., M.D. Moran, E. Solazzo, R.C. Gilliam, V. Matthias, R. Bianconi, K.W. Appel, C. Chemel, J. Ferreira, A.B. Hansen, M. Prank, A. Segers, J.D. Silver, J. Werhahn, R. Wolke, S.T. Rao, and S. Galmarini, 2011: Evaluation of the meteorological forcing used for the Air Quality Model Evaluation International Initiative. *Atmos Environ.* **Submitted for AQMEII Special Issue**

Velden, Christopher S., Kristopher M. Bedka, 2009: Identifying the Uncertainty in Determining Satellite-Derived Atmospheric Motion Vector Height Attribution. *J. Appl. Meteor. Climatol.*, **48**, 450–463.

Vukovich, F.M., Scarborough, J., 2005. Aspects of ozone transport, mixing, and chemistry in the greater Maryland area. *Atmos. Environ.*, 39, 7008-7019.

Wilks, D. S., 1995: *Statistical Methods in the Atmospheric Sciences*. Academic Press, 467 pp.

Wolff, G.T., P.J. Lioy, G.D. Wight, R.E. Meyers and R.T. Cederwall, 1977: An investigation of long-range transport of ozone across the midwestern and eastern U.S., *Atmos. Environ.* **11**, pp. 797–802.

Xiao, Q., E. Lim, D-Y. Won, J. Sun, W-C Lee, M-S Lee, W-J Lee, J-Y Cho, Y-H Kuo, D.M. Barker, D-K Lee, H-S Lee, 2008: Doppler Radar Data Assimilation in KMA's Operational Forecasting. *Bull. Amer. Meteor. Soc.*, **89**, 39–43.

Zhang, D., Zhang, S., Weaver, S.J., 2006. Low-level jets over the mid-Atlantic states: Warm season climatology and a case study. *J. App. Meteor. Clim.*, 45, 194-209.

Zhang, K., Mao, H., Civerolo, K., Berman, S., Ku, J.Y., Rao, S.T., Doddridge, B., Philbrick, C.R., Clark, R., 2001. Numerical investigation of boundary layer evolution and nocturnal low-level jets: local verus non-local PBL schemes. *Environmental Fluid Mechanics*, 1, 171-208.

Zhang, J., Rao, S.T., 1999. The role of vertical mixing in the temporal evolution of ground-level ozone concentrations. *J. of Appl. Meteor.*, 38, 1674-1691.

Xiu, A., and J. E. Pleim, 2001: Development of a Land-surface Model. Part I: Application in a Mesoscale Meteorological Model. *J. Appl. Meteor.*, **40**, 192-209.

List of Tables

Table 1 Comparison of observations from different platforms that are in close proximity (<75 km). Statistics are provided at vertical model levels that are approximately 400, 700 and 1000 m. Numbers in parentheses are the count of site pairs that were used to derive the statistics.

List of Figures

Figure 1 10 m wind speed error (squares) and bias (circles) of the original AQMEII simulation that used surface analysis nudging of wind within the PBL (green) and a test simulation without this surface nudging (red). All statistics include data for the summer of 2006 (Jun-Aug).

Figure 2 Location of various observation sites for each platform. Sites highlighted in blue represent those used for the eastern and western US partitioned statistics in Figure 12.

Figure 3 Observational uncertainty between RAOB and VAD sites as measured by RMSE (wind speed) and MAE (wind direction). These values are computed using RAOB and VAD paired sites that have a spacing of less than 150 km. The circles in the spatial plot are inversely proportional to the site spacing where the largest circles indicate the site pairs that are collocated.

Figure 4 Histograms of layer-average (300-1000 m) wind speed RMSE differences as determined by UHF and VAD sites. These are partitioned by observation network, night/day, and the six sensitivity comparisons.

Figure 5 Spatial plot of the difference in RMSE (wind speed; top) and MAE (wind direction; bottom) between Sensitivity 1 (SENS1) and the base simulation (BASE). Positive (negative) values indicate SENS1 has a larger (smaller) error than BASE. UHF profiler and VAD profiler values are plotted with different symbols as indicated by the legend on the right. The embedded table provides the average error that includes all sites partitioned by platform.

Figure 6 Spatial plot of the difference in RMSE (wind speed; top) and MAE (wind direction; bottom) between Sensitivity 2 (SENS2) and the base simulation (BASE). Positive (negative) values indicate SENS2 has a larger (smaller) error than BASE. UHF profiler and VAD profiler values are plotted with different symbols as indicated by the legend on the right. The embedded table provides the average error that includes all sites partitioned by platform.

Figure 7 Spatial plot of the difference in RMSE (wind speed; top) and MAE (wind direction; bottom) between Sensitivity 3 (SENS3) and Sensitivity 1 (SENS1). Positive (negative) values indicate SENS3 has a larger (smaller) error than SENS1. UHF profiler and VAD profiler values are plotted with different symbols as indicated by the legend on the right. The embedded table provides the average error that includes all sites partitioned by platform.

Figure 8 Spatial plot of the difference in RMSE (wind speed; top) and MAE (wind direction; bottom) between Sensitivity 4 (SENS4) and Sensitivity 1 (SENS1). Positive (negative) values indicate SENS4 has a larger (smaller) error than SENS1. UHF profiler and VAD profiler values are plotted with different symbols as indicated by the legend on the right. The embedded table provides the average error that includes all sites partitioned by platform.

Figure 9 Spatial plot of the difference in RMSE (wind speed; top) and MAE (wind direction; bottom) between Sensitivity 5 (SENS5) and Sensitivity 1 (SENS1). Positive (negative) values indicate SENS5 has a larger (smaller) error than SENS1. UHF profiler and VAD profiler values are plotted with different symbols as indicated by the legend on the right. The embedded table provides the average error that includes all sites partitioned by platform.

Figure 10 Spatial plot of the difference in RMSE (wind speed; top) and MAE (wind direction; bottom) between Sensitivity 6 (SENS6) and Sensitivity 5 (SENS5). Positive (negative) values indicate SENS6 has a larger (smaller) error than SENS5. UHF profiler and VAD profiler values are plotted with different symbols as indicated by the legend on the right. The embedded table provides the average error that includes all sites partitioned by platform.

Figure 11 Comparison of the 300-1000 m layer-average RMSE and bias of wind speed and MAE of wind direction for the original AQMEII simulation and the new experimental assimilation. Also provided in the lower left corner of each panel are the platform-averaged statistics. Un-shaded square represent ignored sites that had less than half the maximum number of hourly samples for the period.

Figure 12 Simulated wind speed RMSE and bias as well as wind direction MAE as a function of time of day. The statistics were computed using UHF profiler and VAD profiler observations at three levels (approx. 400, 700 and 1000 m) for the June 1- August 31, 2006 period. The sites used for these statistics are highlighted blue in Figure 2.

Table 1 Comparison of observations from different platforms that are in close proximity (<75 km). Statistics are provided at vertical model levels that are approximately 400, 700 and 1000 m. Numbers in parentheses are the count of site pairs that were used to derive the statistics.

UHF vs. VAD (34)	Wind Speed (m s^{-1})		
Model Level	RMSE	BIAS	IOA
0.89 (~1000m)	2.05	0.67	0.67
0.915 (~700m)	2.15	0.94	0.65
0.935 (~400m)	2.10	1.03	0.63

UHF vs. VAD	Wind Direction (deg)	
Model Level	MAE	BIAS
0.89 (~1000m)	26	1
0.915 (~700m)	25	2
0.935 (~400m)	24	2

RAOB vs. UHF (17)	Wind Speed (m s^{-1})		
Model Level	RMSE	BIAS	IOA
0.89 (~1000m)	1.67	0.00	0.79
0.915 (~700m)	1.61	0.11	0.80
0.935 (~400m)	1.95	-0.05	0.69

RAOB vs. UHF	Wind Direction (deg)	
Model Level	MAE	BIAS
0.89 (~1000m)	19	2
0.915 (~700m)	18	1
0.935 (~400m)	20	3

RAOB vs. VAD (59)	Wind Speed (m s^{-1})		
Model Level	RMSE	BIAS	IOA
0.89 (~1000m)	1.72	0.39	0.79
0.915 (~700m)	1.81	0.50	0.78
0.935 (~400m)	2.08	0.54	0.71

RAOB vs. VAD	Wind Direction (deg)	
Model Level	MAE	BIAS
0.89 (~1000m)	17	1
0.915 (~700m)	17	1
0.935 (~400m)	20	1

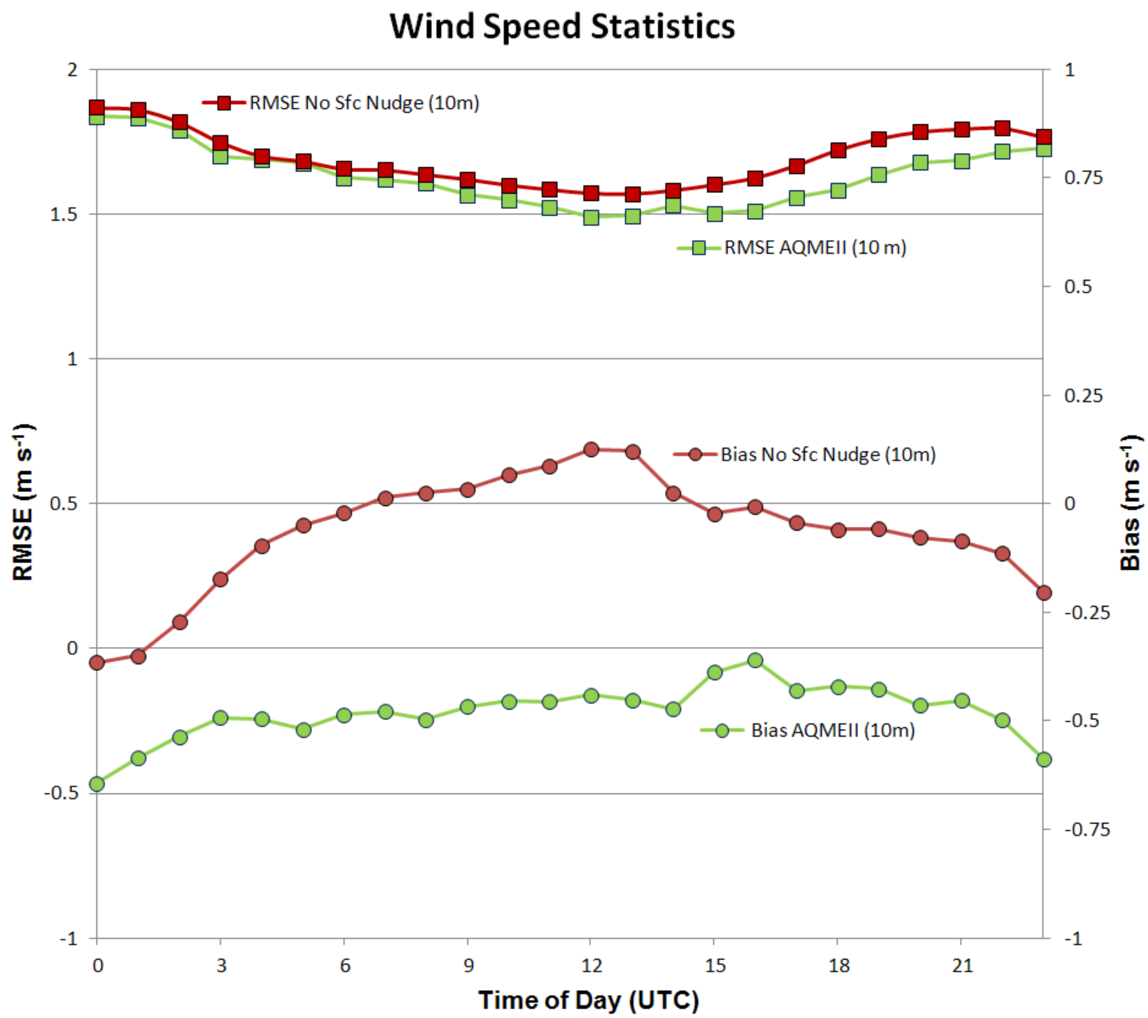

Figure 1 10 m wind speed error (squares) and bias (circles) of the original AQMEII simulation that used surface analysis nudging of wind within the PBL (green) and a test simulation without this surface nudging (red). All statistics include data for the summer of 2006 (Jun-Aug).

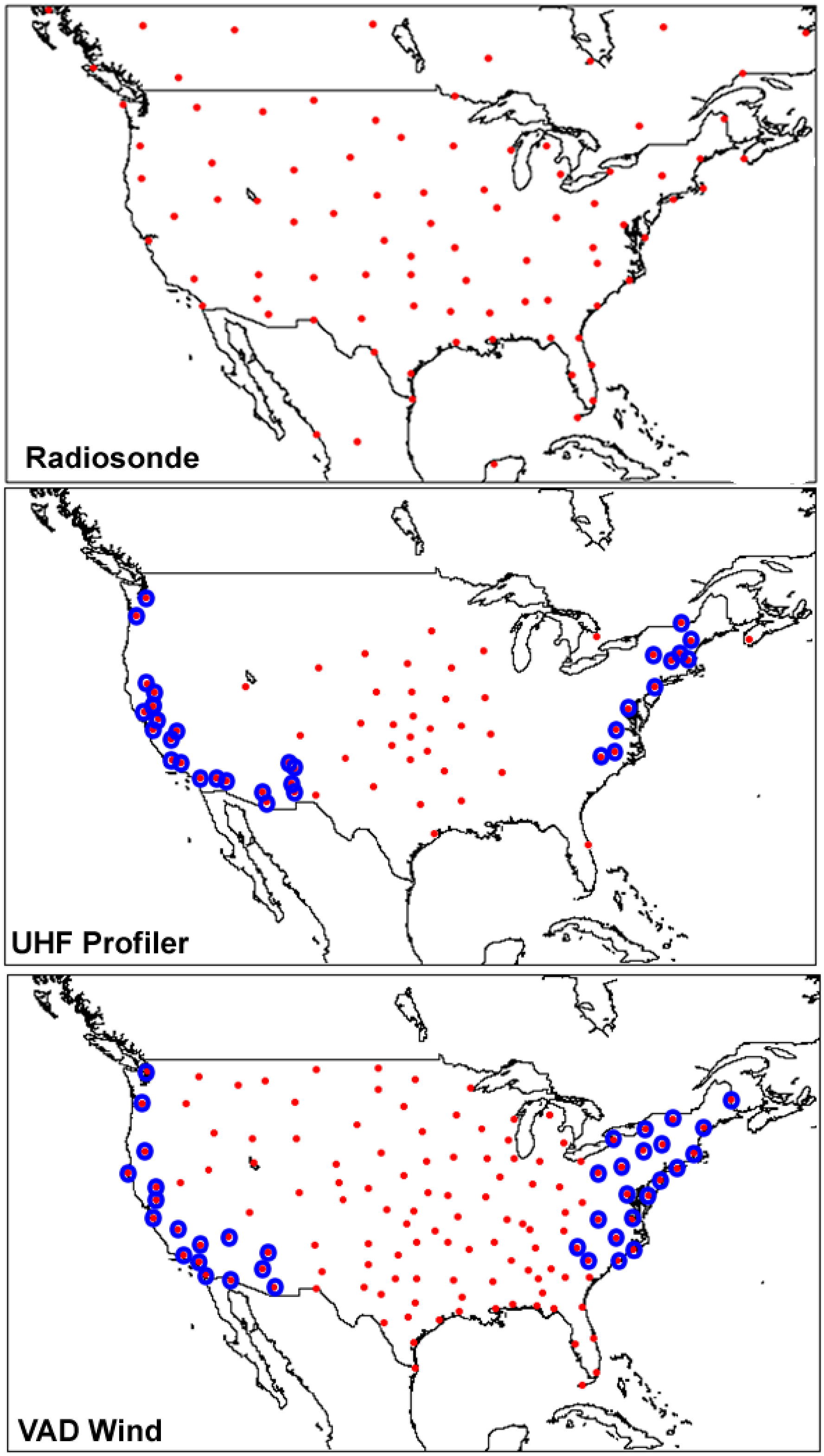

Figure 2 Location of various observation sites for each platform. Sites highlighted in blue represent those used for the eastern and western US partitioned statistics in Figure 12

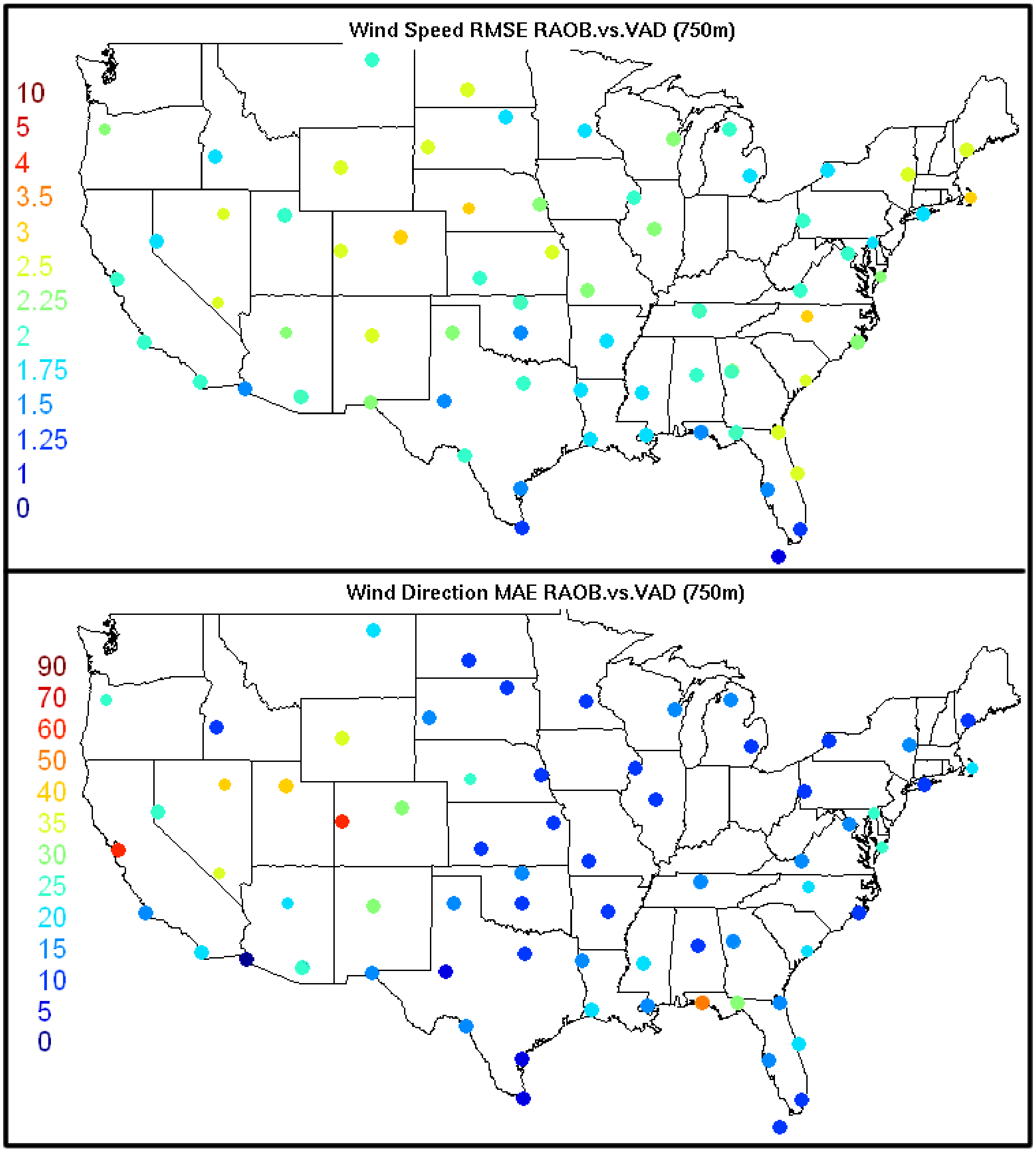

Figure 3 Observational uncertainty between RAOB and VAD sites as measured by RMSE (wind speed) and MAE (wind direction). These values are computed using RAOB and VAD paired sites that have a spacing of less than 150 km. The circles in the spatial plot are inversely proportional to the site spacing where the largest circles indicate the site pairs that are collocated.

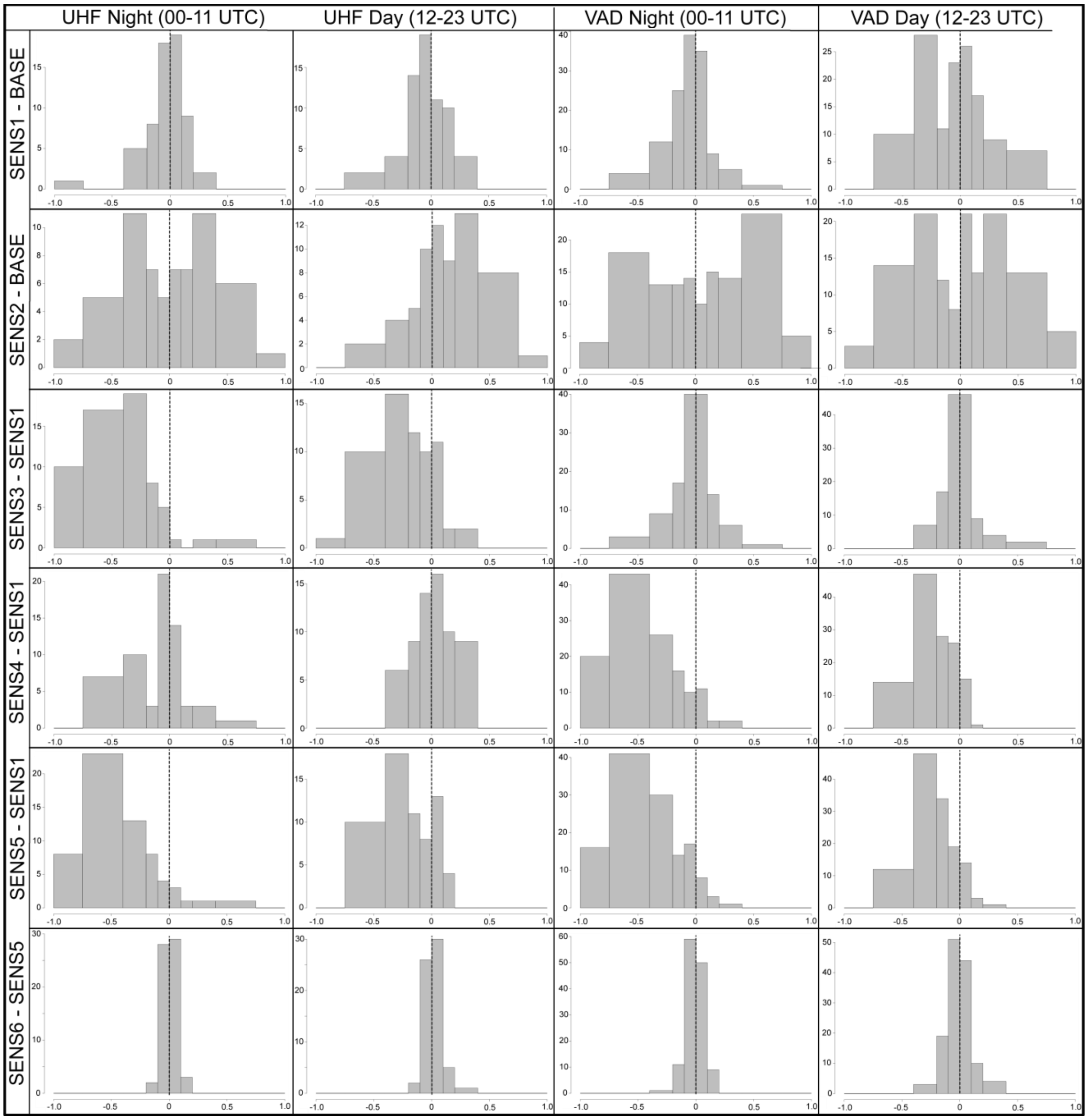

Figure 4 Histograms of layer-average (300-1000 m) wind speed RMSE differences as determined by UHF and VAD sites. These are partitioned by observation network, night/day, and the six sensitivity comparisons.

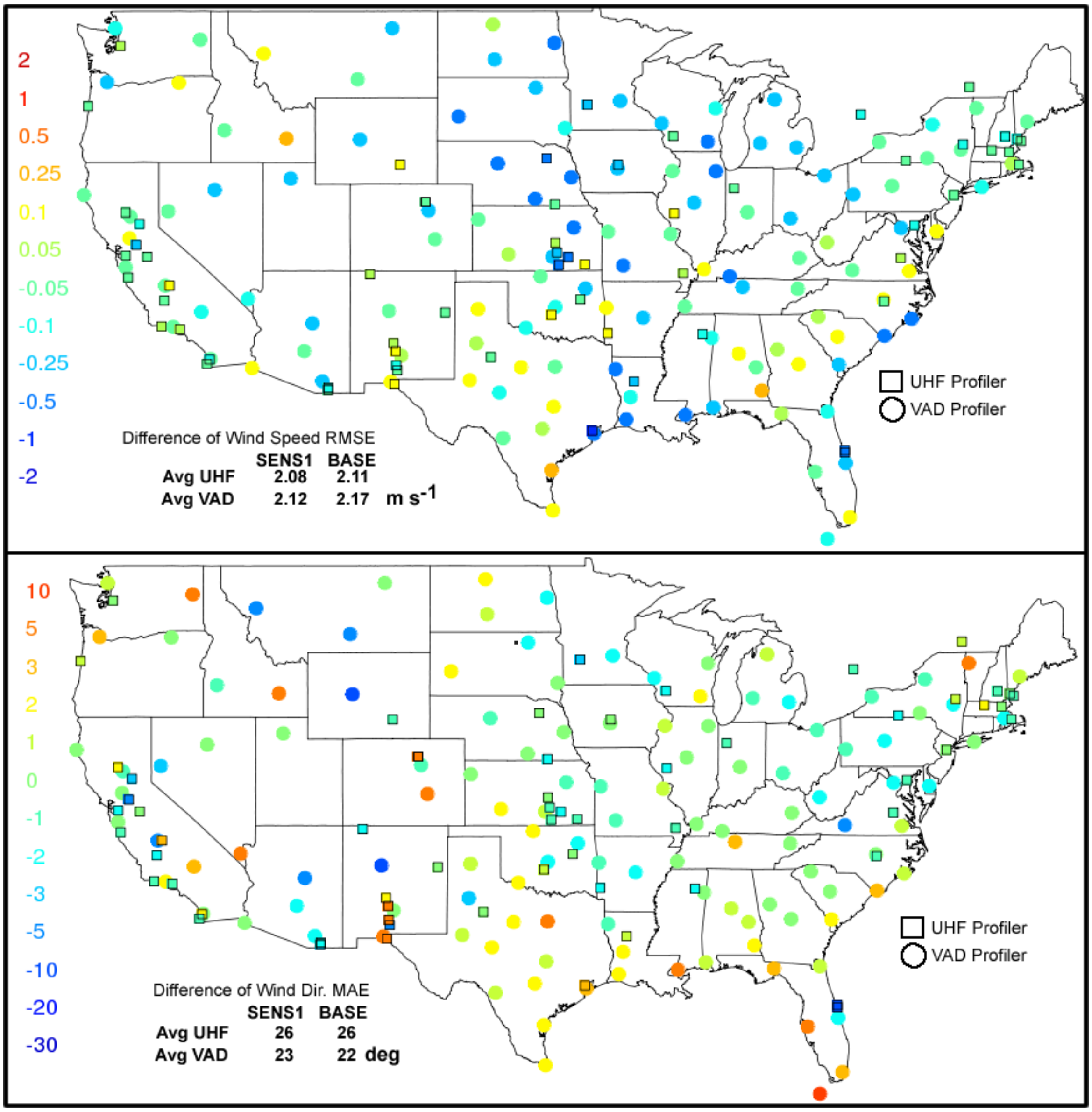

Figure 5 Spatial plot of the difference in RMSE (wind speed; top) and MAE (wind direction; bottom) between Sensitivity 1 (SENS1) and the base simulation (BASE). Positive (negative) values indicate SENS1 has a larger (smaller) error than BASE. UHF profiler and VAD profiler values are plotted with different symbols as indicated by the legend on the right. The embedded table provides the average error that includes all sites partitioned by platform.

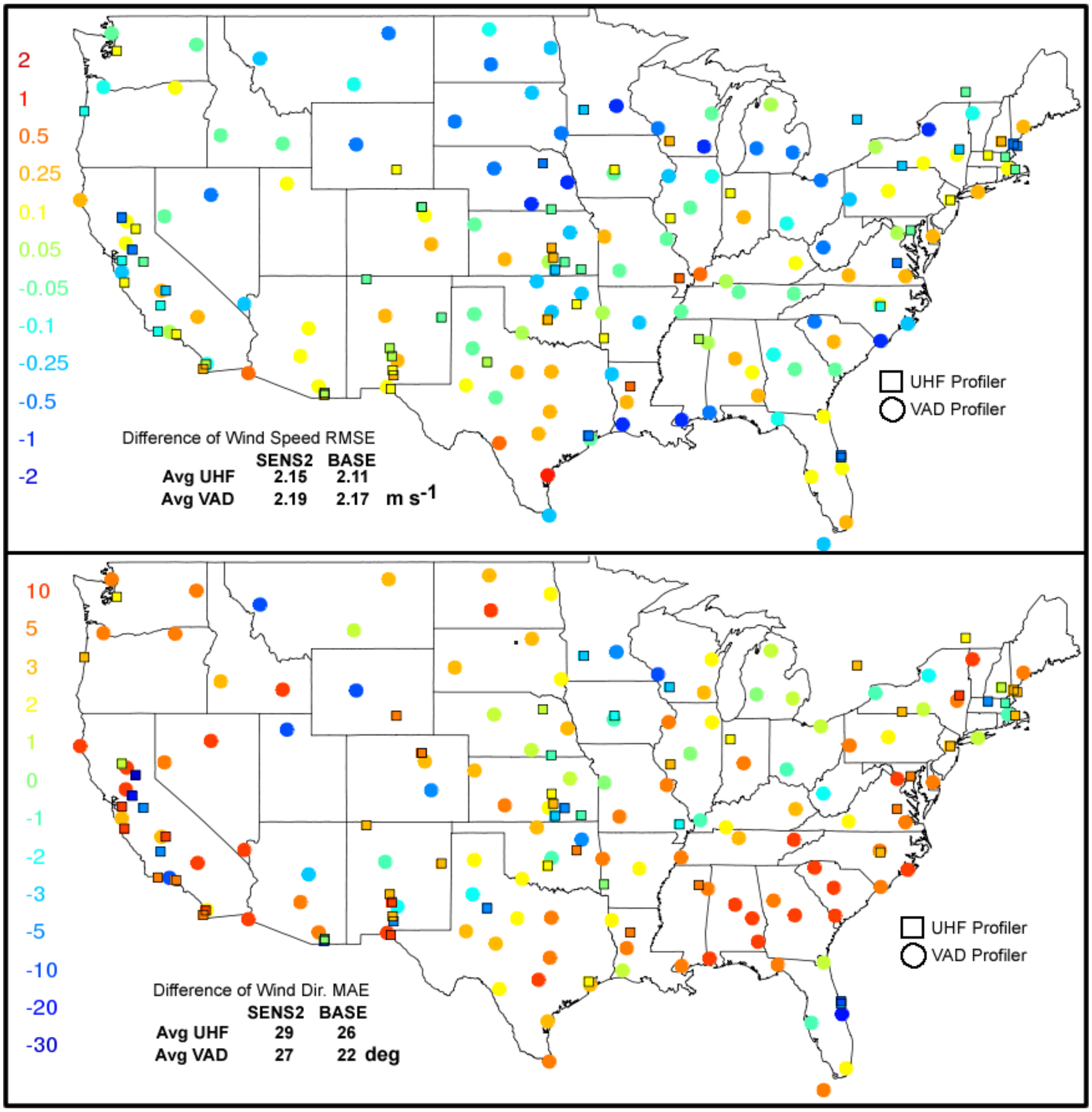

Figure 6 Spatial plot of the difference in RMSE (wind speed; top) and MAE (wind direction; bottom) between Sensitivity 2 (SENS2) and the base simulation (BASE). Positive (negative) values indicate SENS2 has a larger (smaller) error than BASE. UHF profiler and VAD profiler values are plotted with different symbols as indicated by the legend on the right. The embedded table provides the average error that includes all sites partitioned by platform.

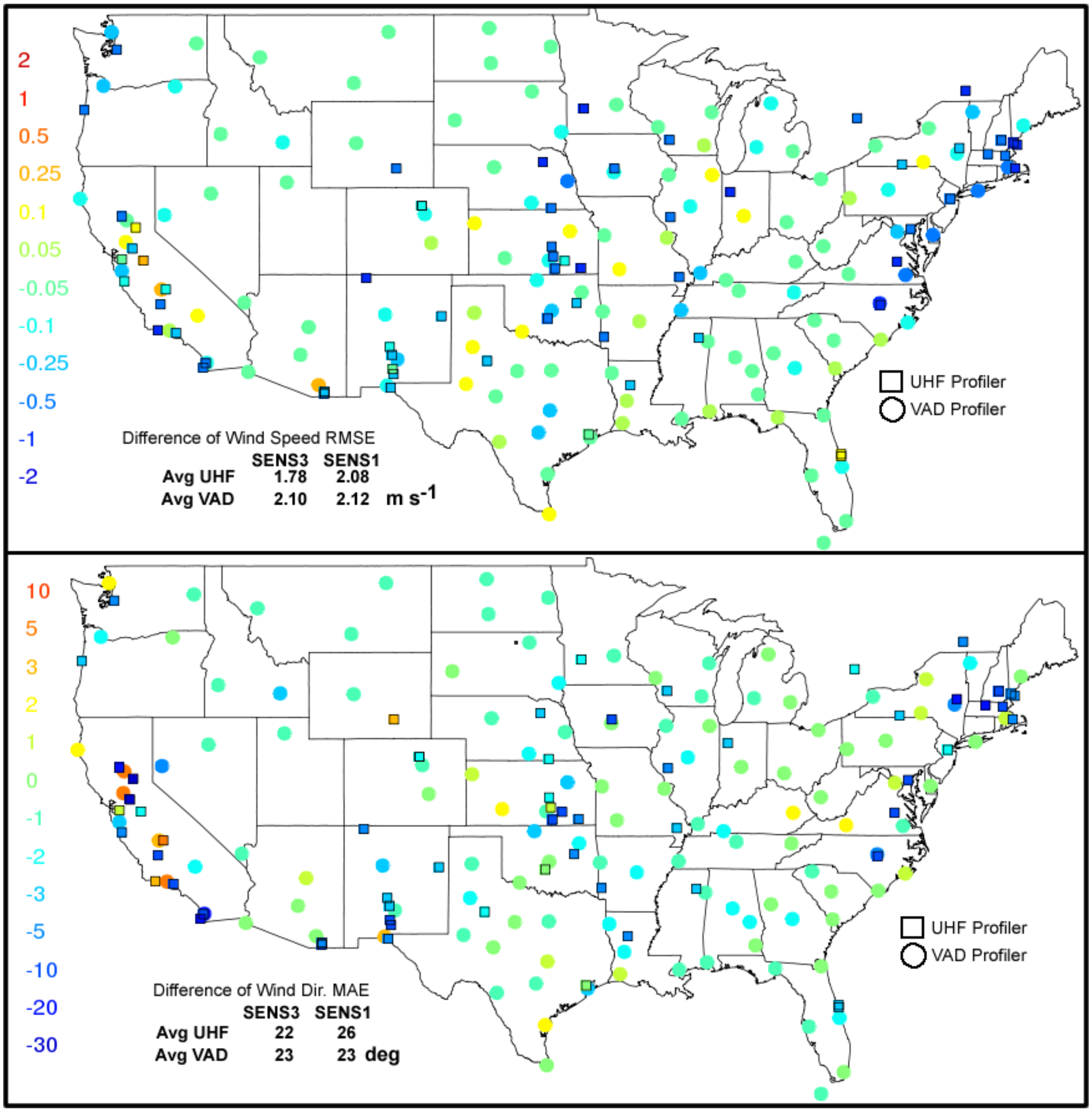

Figure 7 Spatial plot of the difference in RMSE (wind speed; top) and MAE (wind direction; bottom) between Sensitivity 3 (SENS3) and Sensitivity 1 (SENS1). Positive (negative) values indicate SENS3 has a larger (smaller) error than SENS1. UHF profiler and VAD profiler values are plotted with different symbols as indicated by the legend on the right. The embedded table provides the average error that includes all sites partitioned by platform.

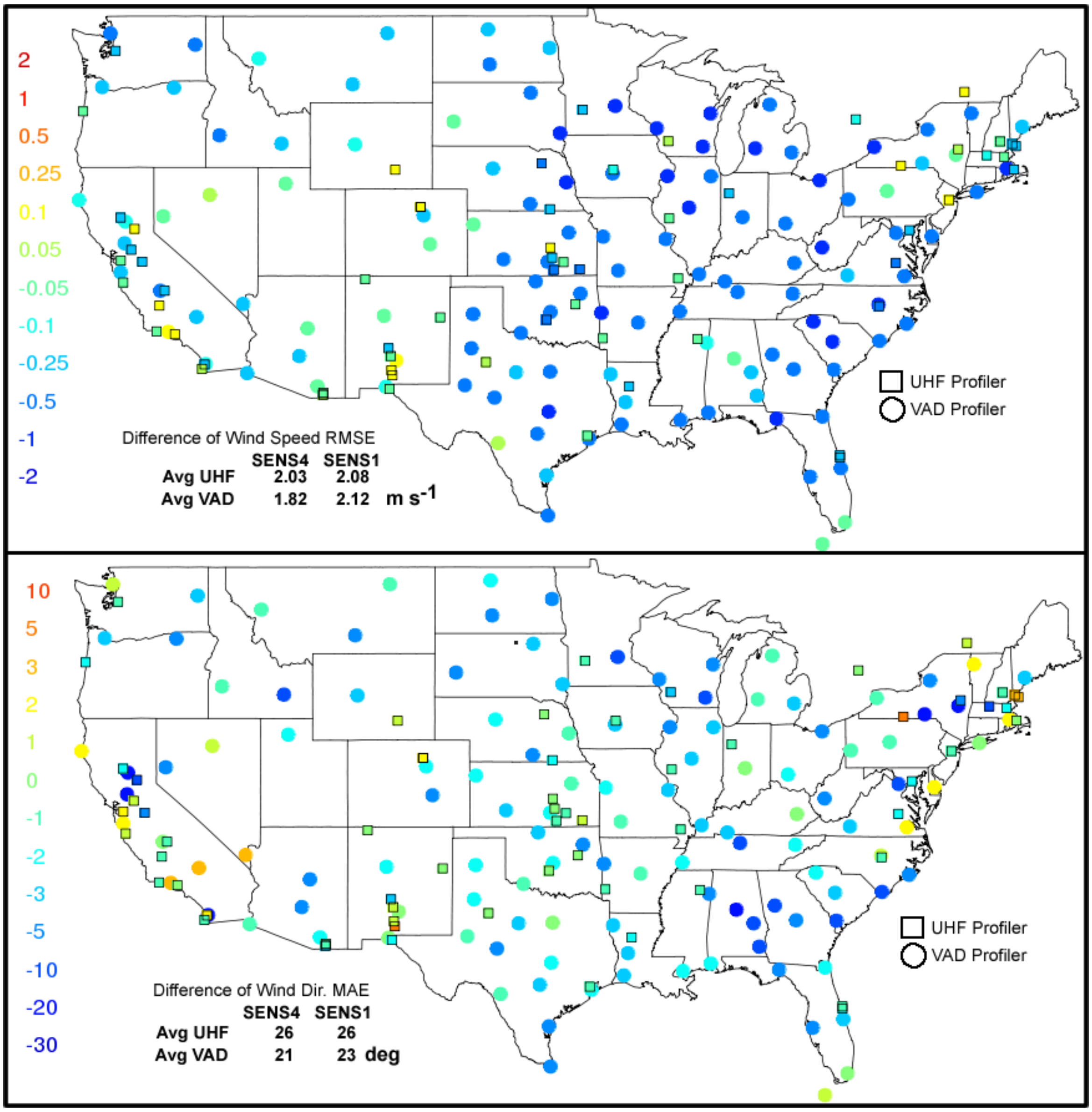

Figure 8 Spatial plot of the difference in RMSE (wind speed; top) and MAE (wind direction; bottom) between Sensitivity 4 (SENS4) and Sensitivity 1 (SENS1). Positive (negative) values indicate SENS4 has a larger (smaller) error than SENS1. UHF profiler and VAD profiler values are plotted with different symbols as indicated by the legend on the right. The embedded table provides the average error that includes all sites partitioned by platform.

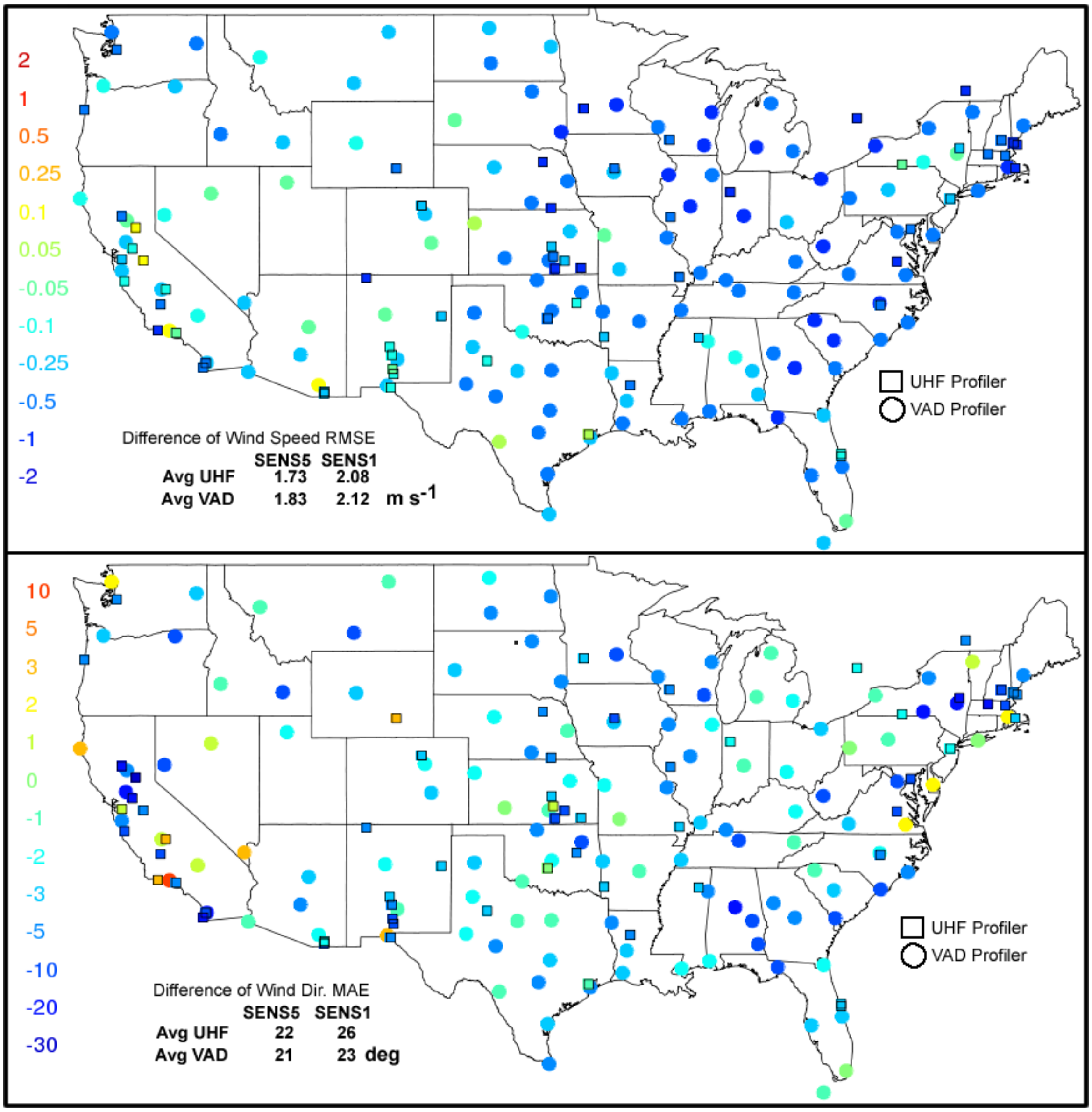

Figure 9 Spatial plot of the difference in RMSE (wind speed; top) and MAE (wind direction; bottom) between Sensitivity 5 (SENS5) and Sensitivity 1 (SENS1). Positive (negative) values indicate SENS5 has a larger (smaller) error than SENS1. UHF profiler and VAD profiler values are plotted with different symbols as indicated by the legend on the right. The embedded table provides the average error that includes all sites partitioned by platform.

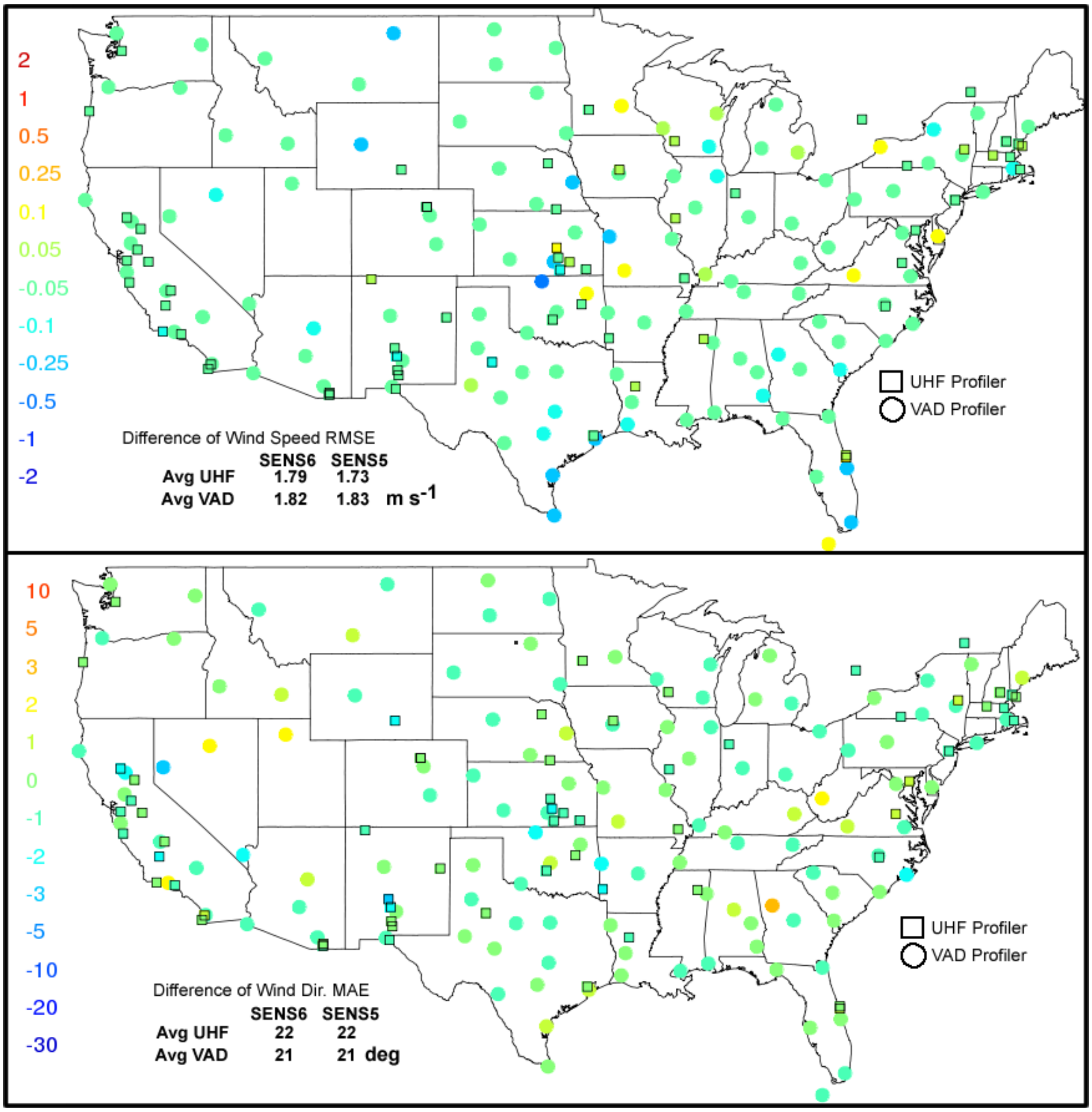

Figure 10 Spatial plot of the difference in RMSE (wind speed; top) and MAE (wind direction; bottom) between Sensitivity 6 (SENS6) and Sensitivity 5 (SENS5). Positive (negative) values indicate SENS6 has a larger (smaller) error than SENS5. UHF profiler and VAD profiler values are plotted with different symbols as indicated by the legend on the right. The embedded table provides the average error that includes all sites partitioned by platform.

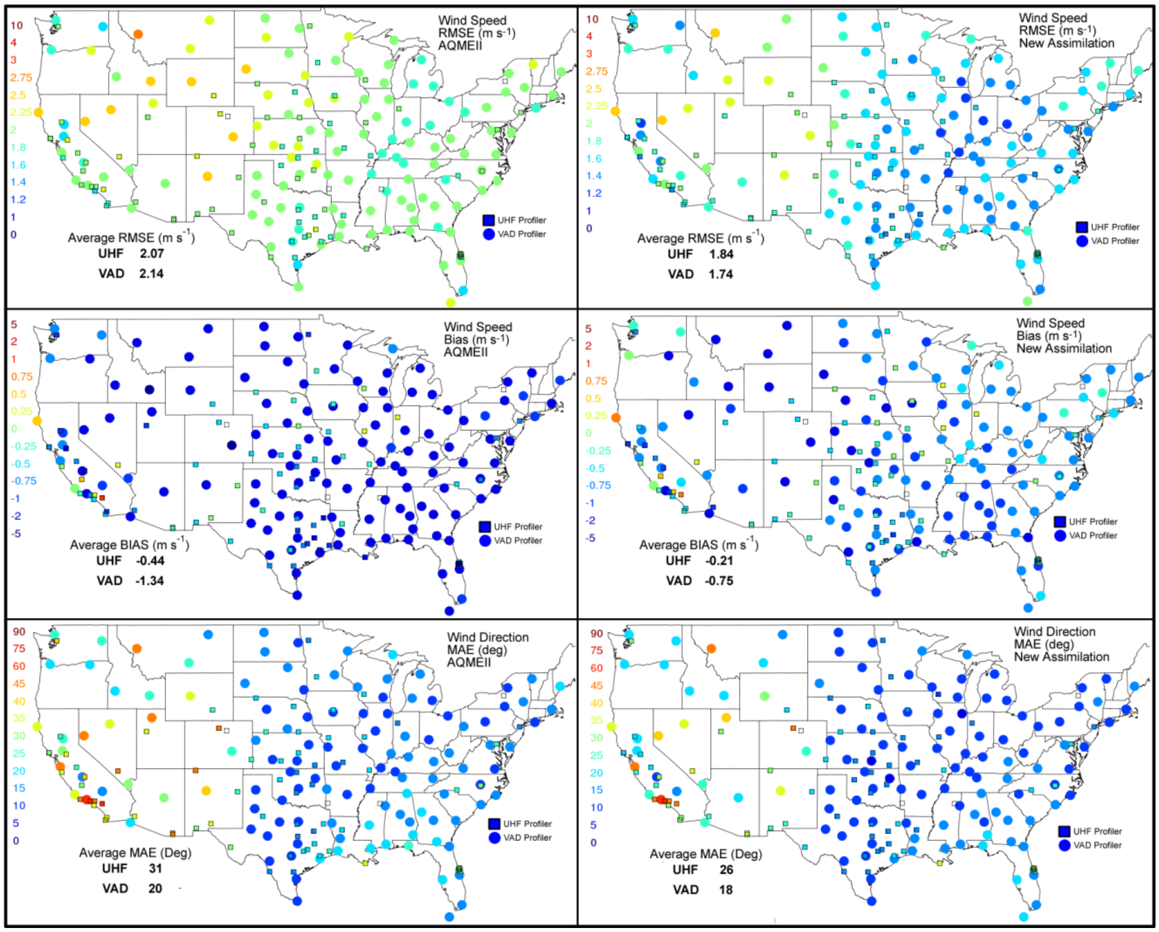

Figure 11 Comparison of the 300-1000 m layer-average RMSE and bias of wind speed and MAE of wind direction for the original AQMEII simulation and the new experimental assimilation. Also provided in the lower left corner of each panel are the platform-averaged statistics. Un-shaded square represent ignored sites that had less than half the maximum number of hourly samples for the period.

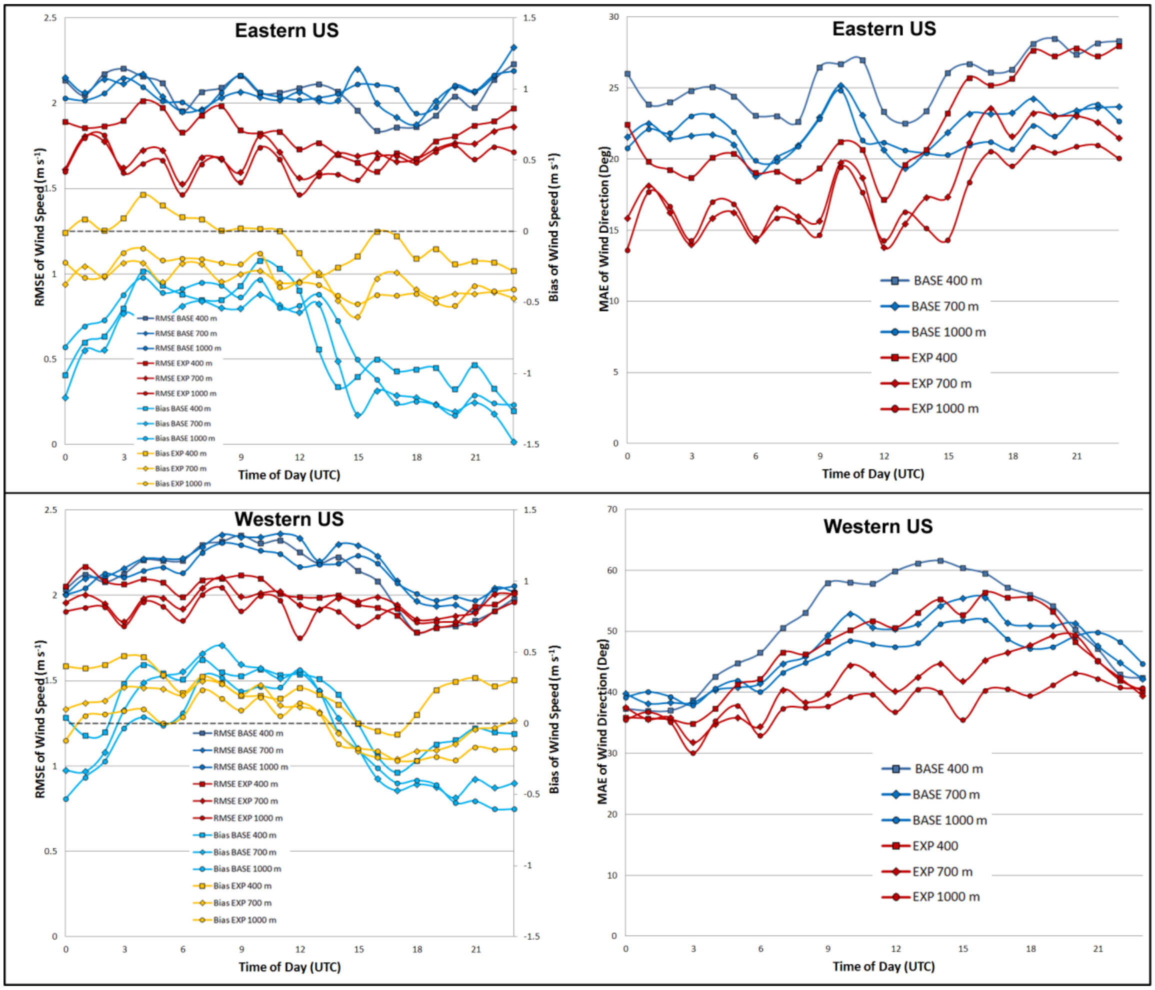

Figure 12 Simulated wind speed RMSE and bias as well as wind direction MAE as a function of time of day. The statistics were computed using UHF profiler and VAD profiler observations at three levels (approx. 400, 700 and 1000 m) for the June 1- August 31, 2006 period. The sites used for these statistics are highlighted blue in Figure 2.